



Global Biogeochemical Cycles

RESEARCH ARTICLE

10.1029/2020GB006564

Key Points:

- We design a general model of unicellular plankton based on size and optimization of trophic strategy traits
- We use the model to predict how the seasonal forcing at different latitudes shapes ecosystem structure and ecosystem functions.
- The adaptive nature of the model makes it particularly well suited for global-scale simulations

Supporting Information:

- Supporting Information S1

Correspondence to:

S. Chakraborty,
sbc@aqua.dtu.dk

Citation:

Chakraborty, S., Cadier, M., Visser, A. W., Bruggeman, J., & Andersen, K. H. (2020). Latitudinal variation in plankton traits and ecosystem function. *Global Biogeochemical Cycles*, 32, e2020GB006564. <https://doi.org/10.1029/2020GB006564>

Received 3 FEB 2020

Accepted 8 JUN 2020

Accepted article online 7 JUL 2020

Latitudinal Variation in Plankton Traits and Ecosystem Function

Subhendu Chakraborty^{1,2} , Mathilde Cadier¹, André W. Visser¹ , Jorn Bruggeman³ , and Ken H. Andersen¹ 

¹Centre for Ocean Life, DTU Aqua, Technical University of Denmark, Copenhagen, Denmark, ²Now at Marine Biological Section, Department of Biology, University of Copenhagen, Copenhagen, Denmark, ³Plymouth Marine Laboratory, Plymouth, UK

Abstract Planktonic ecosystems are usually modeled in terms of autotrophic and heterotrophic compartments. However, the trophic strategy of unicellular organisms can take a range of mixotrophic strategies with both autotrophic and heterotrophic contributions. The dominant emerging strategy found in nature depends on the environment (both biotic and abiotic aspects) and the cell size and influences key ecosystem functions like trophic transfer and carbon export. Ecosystem models that faithfully represent this diversity of trophic strategies are lacking. Here we develop a trait-based model of unicellular plankton with cell size as the master trait and three other traits that determine trophic strategies: investments in photosynthesis, nutrient uptake, and phagotrophy. This unicellular model spans the entire auto- mixo-hererotrophic strategy continuum and the entire size range of unicellular organisms. The model reproduces observed latitudinal patterns in biomass, primary productivity, vertical carbon export, and energy transfer efficiency; all increase with increasing latitude. The size range of mixotrophic cells is independent of the season at low latitudes. At high latitudes, the dominance of pure phototrophs during early spring restricts mixotrophic behavior to a narrower range of cell sizes and with the occurrence of relatively smaller mixotrophs during summer. The model's ability to adapt to different environmental conditions, combined with its simple conceptual structure and low number of parameters and state variables (10), makes it ideally suited for global simulation studies under changing environmental conditions.

Plain Language Summary Marine plankton are important producers in the global biosphere, to the extent that they fuel nearly all marine life as well as impacting global cycling of carbon. How plankton affect ecosystem functions depends on their community structure; how they are distributed in terms of size, how they acquire nutrients, and how they feed off each other. We have developed a new type of model based on a broad description of the possible characteristics and functions of individual plankton cells that can predict unicellular plankton community structure as selected for in different environmental settings. Armed with this model we can simulate key ecological functions—primary productivity, carbon export to deep water, and energy transfer to higher trophic levels—over annual cycles and across the global ocean.

1. Introduction

One of the major environmental forces driving plankton ecosystem on the global scale is the amplitude of the seasonal variation in solar radiation. This seasonal variation increases from the equator to the poles with relatively large amounts of radiation all year at low latitudes to the more oblique angle of the Sun's rays together with long periods of darkness in the winter at high latitudes. This variation impacts the water column physics, in particular its stratification, with equatorial regions being permanently stratified while in temperate and polar regions, winters break down the stratification to be reestablished the following spring. These are fundamental drivers of plankton community structure and function, with equatorial (stratified) systems tending to be oligotrophic with high nutrient recycling, less export of organic material to the deep ocean, and little transfer of energy to higher trophic levels, while higher latitude systems are increasingly eutrophic, at least in winter/spring, with less recycling, higher export to the deep ocean, and higher transfer of energy to higher trophic levels (Friedland et al., 2012; Ryther, 1969). A complicating factor is how much of these differences are due to differences in temperature rather than light. Much effort has been invested in understanding the effects of temperature on the physiology of plankton (Eppley, 1972; Li, 1985); however, as the variation in seasonal amplitude correlates strongly with temperature, it is difficult to disentangle

the effects of temperature from those of the seasonal amplitude. One way to isolate the effects of seasonal variation from those of temperature is in simplified model systems. One problem, though, is that the species and types of plankton organisms will be very different in tropical and polar systems. The model, therefore, needs to be sufficiently flexible to describe the emerging community structure in both regions.

Trait-based modeling approaches manage to be both adaptive and have a small set of parameters, which are not region-specific (Bruggeman & Kooijman, 2007; Ward & Follows, 2016). Trait-based models are based upon key traits that define the fitness of organisms for given biotic and abiotic conditions (Litchman & Klausmeier, 2008; Westoby & Wright, 2006). The fitness of organisms can vary along environmental and biological gradients, resulting in characteristic temporal and spatial distribution of traits. In this way, the expression of traits according to environmental variations potentially makes trait-based models applicable across a broad range of oceanic systems. Trait-based models are therefore able to describe ecosystems across the entire range of latitudinal differences in seasonal forcing.

The simplicity of trait-based models depends on the careful selection of key traits and a formulation upon trade-offs between traits and vital rates (Kiørboe et al 2018). Cell size has been found as one of the most important traits of plankton (Kiørboe & Hirst, 2014; Litchman & Klausmeier, 2008; Marañón, 2015) and is commonly used in plankton ecosystem models (Acevedo-Trejos et al., 2018; Banas, 2011; Terseleer et al., 2014; Ward et al., 2012). Size affects most relevant functions of plankton, for example, resource affinity, respiration rates, maximal growth rate, and uptake rates (Andersen et al., 2016; Chisholm, 1992; Edwards et al., 2012). Further, the mortality risk associated with predation (grazing) is higher in small size organisms, giving larger organisms an advantage over smaller ones when predators are abundant (Thingstad et al., 2005). Due to the size-related dependency of access to the different resources for planktonic organisms, trophic strategies and adaptive choices related to environmental biotic and abiotic conditions vary systematically with size (Andersen et al., 2015; Chakraborty et al., 2017).

In addition to cell size, the trophic strategy is also an important trait within unicellular plankton. Most plankton models divide plankton into two fundamental groups: autotrophs and heterotrophs, usually designated as phytoplankton and zooplankton respectively. This division, however, is challenged by the recent realization of the dominance of mixotrophs that combine phototrophy with phagotrophy (eating particulate organic matter) among unicellular plankton (Flynn et al., 2013). Mixotrophs are found almost everywhere in the illuminated water column, both in freshwater and marine environments (Hartmann et al., 2012; Sanders, 1991; Stoecker et al., 2009), oligotrophic and eutrophic systems (Burkholder et al., 2008), and from polar to equatorial regions (Sanders & Gast, 2012; Stoecker et al., 2009; Zubkov & Tarran, 2008). Because of their flexibility in nutritional modes and their ability to deal with low inorganic nutrients levels by sourcing organic carbon and nutrients from other organisms, mixotrophs compete successfully with specialists and contribute to the export of organic matter toward higher trophic levels (Ward & Follows, 2016). Thus, within the unicellular plankton communities of the world's oceans, a range of trophic strategies, from pure phototrophy over various degrees of mixotrophy to pure heterotrophy, exists and requires a realistic representation in biogeochemical plankton model to replace the traditional division between phytoplankton and zooplankton (Andersen et al., 2015).

Here we develop a dynamic trait-based modeling framework of unicellular plankton that accounts for both cell size and trophic strategies of plankton. The model is based on the optimization framework by Chakraborty et al. (2017), which is expanded to a fully dynamic model. The model uses cell size as the master trait. Within each size group, investments determine three traits that describe the trophic strategy: phototrophy (investment in light-harvesting), nutrient acquisition (investment in machinery for the uptake of external dissolved nutrients), and phagotrophy (investment in the capture and digestion of smaller cells). The model is implemented in a water column and describes the seasonal variation of community structure and trophic strategies of different size classes of plankton across latitudes.

We use the model to understand the differences in plankton ecosystem structure and function across latitudes, from the tropical ocean to subpolar regions. We demonstrate a rather abrupt transition around 40°N, below which the seasonal forcing is unable to break down stable stratification. Due to the seasonal break down of the stratification at higher latitudes, the model leads to increased biomass, primary productivity, vertical carbon export to deep water, and higher energy transfer efficiency to higher trophic levels. Mixotrophic size range is independent of the season at low latitudes, whereas at high latitudes, the

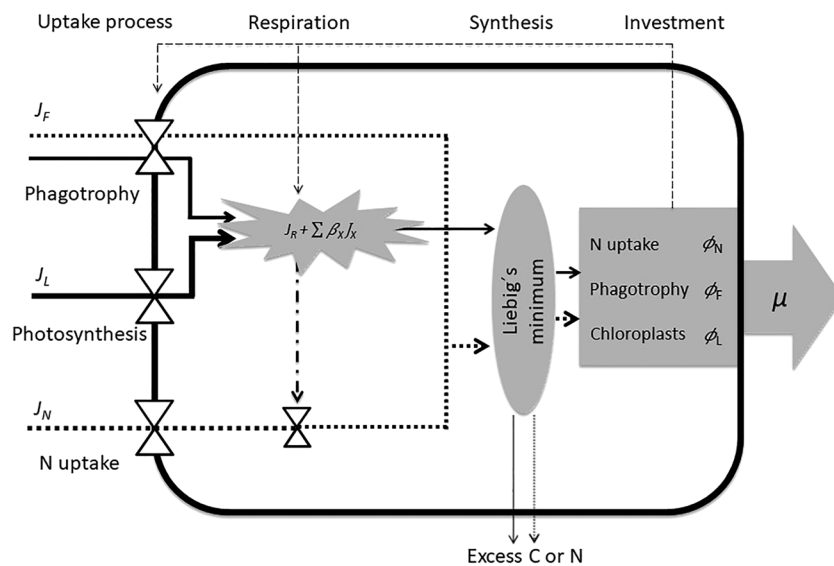


Figure 1. Schematic representation of carbon (solid lines) and nitrogen (dotted lines) fluxes in a cell. The thin dashed lines illustrate how the investment in photoharvesting (ϕ_L), nutrient uptake (ϕ_N), and phagotropy (ϕ_F) influence uptakes and respiration.

mixotrophic behavior is restricted to a narrower range of cell sizes with the occurrence of relatively smaller mixotrophs during summer. These results emphasize the ability of our trait-based model to capture the changes in community composition and associated ecosystem functions over a gradient of physical and biogeochemical conditions using optimization of a small number of traits within size classes.

2. Methods

2.1. Overview of the Cell Model of Unicellular Plankton

The model represents cells of different size classes that (1) produce organic carbon through photosynthesis (J_L), (2) obtain dissolved inorganic nitrogen from the external medium (J_N), and (3) obtain organic carbon and nitrogen through phagotropy (J_F) (Figure 1). Uptake of resources is regulated by investments in resource harvesting options and subjected to size-based constraints. These investments are optimized to always produce the highest population growth rate. The key assumptions lie in the relations between investments of resource uptakes and cell size. These assumptions follow Chakraborty et al. (2017). The model accounts for acquired carbon and nutrients to ensure that the cell satisfies its needs for both. While photosynthesis and nutrient uptake provide carbon and nitrogen, cells also obtain both carbon and nitrogen from prey organisms through phagotropy. Carbon obtained from photosynthesis and phagotropy is respired in the process of resource uptake, building and maintaining of organelles (explosion symbol in Figure 1), and for standard metabolism. Due to the carbon costs of nutrient uptake, the cell will downregulate this uptake when carbon from the photosynthetic pathway is limiting (dashed-dotted line in Figure 1; Appendix B). This process represents a second layer of optimization. The synthesis of biomass from the remaining available carbon and nitrogen follows Liebig's law of the minimum (gray ellipse in Figure 1) and is constrained by the Redfield ratio (mass C:N ratio = 5.68; Redfield, 1958). In this process, the excess assimilated carbon or nutrient is excreted from the cell. Cell division rate μ_i is then found as the mass-specific synthesis rate. The remainder of the model is a fairly standard description of bioenergetics and mass balancing with size-based predator-prey interactions (Banas, 2011; Ward & Follows, 2016). The cell model is embedded in a hydrodynamic model that represents physical properties of the water (light and diffusion) and controls the vertical mixing of biotic and abiotic variables. In the following, we go through the main assumptions and equations in the cell model, with the details in Appendices A–C. The hydromechanical model is only briefly sketched out and detailed in Appendix D.

2.2. Cell Representation

Cells are characterized by their size, x ($\mu\text{g N cell}^{-1}$), and their investments (ϕ_X) in uptake processes. The investments represent organelles and enzymes associated with the uptake processes of photosynthesis ϕ_L (including pigments and enzymes for carbon fixation), nutrient uptake ϕ_N (including enzymes for reduction of nitrate to ammonium and transmembrane porters), and phagotrophy ϕ_F (including the membrane material for food vacuole formation and digestive enzymes) (Berge et al., 2017; Chakraborty et al., 2017). The investment traits measure the investment relative to the structural biomass and therefore dimensionless numbers with values between 0 and 1. In addition, a fraction ϕ_m of the cell is occupied by cell membranes. Following Clark et al. (2013), we can calculate ϕ_m by considering the membrane consisting of an outer membrane and a cytoplasmic membrane, with a periplasm between the two membranes. As the thicknesses of each of these membranes are independent of the cell size, the fraction ϕ_m can be calculated (see Appendix A). As cells become smaller, the membranes take up an increasing fraction of the total mass, leaving less space for investments and structural biomass (Figure A1). The total biomass x ($\mu\text{g N cell}^{-1}$) is thus divided between structural biomass, the investment traits, and the membrane:

$$\phi_L + \phi_N + \phi_F + \phi_m(x) = 1, \quad (1)$$

where the membrane fraction is a fixed function of size, while the other investments will be determined dynamically by optimization.

2.2.1. Uptake of Resources

The uptake of a resource X (light/carbon L , inorganic nitrogen N , or prey F) is determined by an affinity A_X for the resource and a maximum uptake rate $J_{\max,X}$. Both parameters are determined by the investments (ϕ_X) in concert with cell size. Investment in resource uptake confers a benefit in terms of a higher affinity toward the resource and a higher maximum uptake rate. We assume that at low investments the affinity increases linearly with the investment, which ensures that the affinity goes to zero when the investment is zero. At high investments, however, the affinity becomes limited due to physical constraints related to cell size. The interaction between the investments and the limiting process is described by a simple saturating function:

$$A_X = A_{\max,X}(x) \frac{\alpha_X \phi_X x}{\alpha_X \phi_X x + A_{\max,X}(x)}, \quad (2)$$

where α_X is the affinity gained per investment $\phi_X x$. The affinity scales linearly with investment for small investments ($\phi \ll A_{\max}/(\alpha x)$) and small cells ($x \ll A_{\max}/(\alpha \phi)$). The physical constraints, which determine the maximum affinities, $A_{\max,X}$, vary with the type of resource (Andersen et al., 2015):

Light harvesting is limited by self-shading of pigments inside the cell (the package effect; Finkel & Irwin, 2000; Morel & Bricaud, 1981). This means that at high investments, photosynthesis is effectively limited by the cell surface, which scales with mass as $\propto x^{2/3}$. For this reason, we can write $A_{\max,L}$ as

$$A_{\max,L} = c_L x^{2/3}. \quad (3)$$

where c_L is a constant which determines the combination of investment and cell size where the surface limitation takes effect. This scaling of maximum affinity with cell size is generally observed in meta-analyses across species, for example, Edwards et al. (2015).

Under low nutrient concentrations, cells cannot absorb nutrients faster than they diffuse toward the cell, a process that is physically limited by the radial dimension of a cell (Munk & Riley, 1952). As a result, the diffusion-limited affinity for nutrients scales as $\propto x^{1/3}$ (Munk & Riley, 1952). This limitation is represented by writing $A_{\max,N}$ as

$$A_{\max,N} = c_N x^{1/3}. \quad (4)$$

where c_N is a constant. Small cells tend to become limited by the ability to take up nutrients. Uptake limitation results in the scaling of affinity with cell surface or cell mass. The transition between the 1/3

scaling of nutrient affinity for large cells and the linear scaling for small cells is represented by Equation 2 and was demonstrated in the meta-analysis by Lindemann et al. (2016).

Predation on smaller cells (phagotrophy) is shown empirically to scale linearly with cell volume (\propto) (Kiørboe, 2011). Thus, the maximal affinity for phagotrophy, $A_{\max,F}$, can be written as

$$A_{\max,F} = c_F x. \quad (5)$$

This means that there is no limitation by cell size for phagotrophy, and the affinity just scales linearly with size and investment.

Investments in resource uptakes also increase maximum uptake rates. The maximum uptake rates play dual roles in the model by representing both maximum uptake rates and maximum biosynthesis rates. Maximum uptake rates are limited by processing machinery, such as chloroplasts, nutrient transporters, organelles, and enzymes involved in digestion. We assume that the capacities of these machinery scale linearly with investments and therefore maximum uptake rates are not, as are the affinities, constrained by physical restrictions and do not saturate at high investments. They are only limited by their trade-off with other investments (Equation 1). The maximum uptake rates are therefore simply proportional to the investments:

$$M_X = m_X \phi_X x, \quad (6)$$

where m_X is the maximum uptake rate per investment. The linear scaling of maximum uptake rates with size means that maximum growth rates will also scale linearly with size. Linear scaling of maximum growth rates is commonly observed in the analysis of unicellular plankton, though with a small decline (Edwards et al., 2012) or a maximum around 100 μm (Maranon et al 2013).

With the affinities given by (2) and Equations 3–5 and maximum uptakes by (6), the uptake J_X of resource X is governed by a standard saturating Holling type II functional response (symbolized by large white triangles in Figure 1). For light this is

$$J_L = M_L \frac{A_L L}{A_L L + M_L}. \quad (7)$$

The nutrient uptake contains an additional downregulation of the uptake with a factor $\rho \in [0 : 1]$ (dash-dotted line in Figure 1):

$$J_N = \rho M_N \frac{A_N N}{A_N N + M_N}. \quad (8)$$

This factor represents that the cell might downregulate the nutrient uptake due to the carbon costs of the uptake. This downregulation is modeled as an optimization process (Appendix B). This optimization is similar to the flux balance analyses used in bio-engineering (Orth et al., 2010).

Phagotrophic uptake is regulated by a similar functional response as light and nutrient uptakes. It is, however, adjusted by prey switching, whereby predatory cells feed preferably on the size classes with higher abundances. This process is explained with the description of the full plankton ecosystem in section 2.2.4.

2.2.2. Respiration and Biosynthesis

Respiration fuels the uptake of resources, maintenance of investments, and basal metabolism. Assimilation cost of each resource is proportional to the uptake: $\beta_X J_X$, with a constant β_X . Maintaining organelles is proportional to the investment: $r_X \phi_X x$, where r_X is a constant. Basal metabolism is proportional to mass: $r_0 x$ with r_0 being the costs per mass. The metabolic costs are then

$$J_R = r_0 x + \sum_X \beta_X J_X + \sum_X r_X \phi_X x. \quad (9)$$

The assimilated carbon, nutrients, and food are combined toward synthesizing new structure and investments. Different investments could have different C:N ratios, but here we assume that the structure, investments, and assimilated food all have the same C:N ratio, c_{CN} (units of $\mu\text{g C}/\mu\text{g N}$). The total available C and N

are $(1 - \beta_L)J_L + (c_{CN} - \beta_F)J_F - \beta_N J_N - J_R$ and $J_N + J_F$, respectively. The combination of C and N is performed following Liebig's law of the minimum (units of $\mu\text{g N/day}$):

$$J_{\text{tot}} = \min \left[\frac{(1 - \beta_L)J_L + (c_{CN} - \beta_F)J_F - \beta_N J_N - J_R}{c_{CN}}, J_N + J_F \right]. \quad (10)$$

Here J_L is given in units of $\mu\text{g C/day}$, whereas, J_N and J_F are given in $\mu\text{g N/day}$. J_{tot} is the flux of nutrients (and carbon) available for synthesis. Note that the synthesis does not involve a limiting maximum synthesis capacity; limitation of synthesis is taken care of by the limitation of uptake of light, nutrients, and food in the functional responses (Equations 7, 8, and 16). The division rate of the cells follows directly as (day^{-1})

$$\mu = J_{\text{tot}}/x. \quad (11)$$

Excess nitrogen will be excreted with the rate

$$N_E = J_F - \max \left[0, \frac{(1 - \beta_L)J_L + (c_{CN} - \beta_F)J_F - J_R}{c_{CN}} \right]. \quad (12)$$

2.2.3. Optimization of Trophic Strategy

Organisms regulate their investments in resource harvesting traits (ϕ_X) to optimize their cell division rate according to the environmental conditions (light, nutrient concentrations, and food availability):

$$\phi^*(X) = \operatorname{argmax}_{\phi} \{\mu(\phi, X)\} \quad (13)$$

where $\phi = \{\phi_L, \phi_N, \phi_F\}$ and $X = \{L, N, F\}$. The optimization is subject to the constraint that the sum of the investments plus the costs of the membrane is less than or equal to 1 (Equation 1). The growth rate of the i th size class is then $\mu^*(X) = \mu(\phi^*, X)$. To avoid making the optimization in (13) at every time step during the simulation, a lookup table of $\mu^*(X)$ over realistic ranges of the three resources (light, nutrient, and food) and two investment traits (light and nutrient) is created at the beginning of the simulation. Specifically, all resources and investment traits are discretized into 30 logarithmically spaced and equispaced intervals, respectively, over their realistic ranges.

The continuous and instantaneous optimization of trophic strategies is a key assumption that makes it possible to simulate the model with cell size as the only trait axis. In a community of plankton cells in the ocean, the process of optimizing trophic strategy occurs on a variety of time scales: time scales of hours via acclimation, for example, photo acclimatization of the investment in light harvesting (Masojídek et al., 1999); time scales of weeks due to demographic sorting, that is, strategies with low division rates are replaced by strategies with high division rates (Smith & Kalf, 1983; Sommer, 1983), and longer evolutionary time scales, that is, genetic changes. The model does not distinguish between these processes but rather represents them all as if there is only one type of cell of each size that has unlimited flexibility to adjust its strategy—as represented by the investments—instantaneously. While the instant optimization assumption accurately represents the process of acclimation at the population level, it is at best an approximation of changes in trophic strategy due to demographic sorting. However, when the process of sorting is slow, such as seasonal to interannual variation, the optimal strategy is a good approximation of the demography change (Terseleer et al., 2014).

2.2.4. Plankton Ecosystem and Predator–Prey Interactions

The ecosystem is represented by the biomass of cells in eight logarithmically spaced size classes based on their cellular nitrogen content ranging from 10^{-7} to $1 \mu\text{g N}$ (~ 1 to $800 \mu\text{m}$ in terms of equivalent spherical diameter). The biomass concentration of the i th size group, with mass x_i , is $P_i (\mu\text{g N L}^{-1})$. We assume that a constant fraction f_B of the detrital pool is bacterial biomass, $B = f_B D (\mu\text{g N L}^{-1})$, with size $x_B = 10^{-9} \mu\text{g N cell}^{-1}$.

The total food availability for predators in size class i (F_i) is

$$F_i = \sum_j \theta_{j,i} P_{j,i} + \theta_{B,i} B, \quad (14)$$

where $\theta_{j,i}$ is the size preference of a predator of size class i for prey size class j (also for bacteria B). The size preference is assumed to be log-normally distributed:

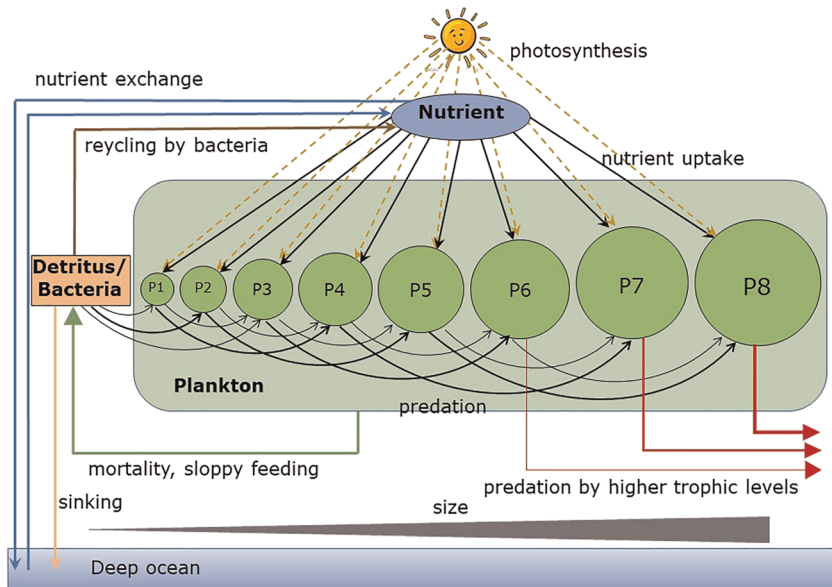


Figure 2. Schematic diagram of the food-web model. The model consists of one nutrient, eight different size classes of plankton (P' s), and detritus/bacteria. The deep ocean represents depths larger than 500 m.

$$\theta_{j,i} = \exp \left[- \left(\log \left(\beta \frac{x_j}{x_i} \right) \right)^2 / (2\sigma^2) \right], \quad (j = 1, 2, \dots, n, B) \quad (15)$$

where β is the preferred predator-prey mass ratio and σ is the niche width. The feeding rate by size class i on prey class j and bacteria B is determined by a functional response similar to Equations 7 and 8, though regulated by prey switching:

$$J_{\text{pred},j,i} = J_{\max,F,i} \frac{A_{F,i} F_i}{A_{F,i} F_i + J_{\max,F,i}} \Theta_{j,i}, \quad (j = 1, 2, \dots, n, B) \quad (16)$$

where the prey switching factor $\Theta_{j,i}$ is determined by the availability of prey and bacteria (Ward & Follows, 2016):

$$\Theta_{j,i} = \frac{(\theta_{j,i} P_j)^2}{\sum_j (\theta_{j,i} P_j)^2 + (\theta_{B,i} B)^2}, \quad (j = 1, 2, \dots, n, B) \quad (17)$$

Clearly, $\theta_{j,i}$ represents predation preference based on prey size whereas $\Theta_{j,i}$ reflects predation preference based on prey biomass.

The total phagotrophic flux into cells in size class i is therefore

$$J_{F,i} = \sum_j J_{\text{pred},j,i}. \quad (j = 1, 2, \dots, n, B) \quad (18)$$

2.3. Ecosystem Dynamics in 1-D Vertical Water-Column

The hydrodynamic model describes the dynamics of dissolved inorganic nutrients (as nitrogen) N ($\mu\text{g N L}^{-1}$), detritus D ($\mu\text{g N L}^{-1}$), and plankton biomass in a 1-D vertical water column (Figure 2). The space-time dynamics of these components are

$$\frac{\partial N}{\partial t} = - \sum_i J_{N,i} \frac{P_i}{x_i} + \sum_i N_{E,i} P_i + \gamma_r D + \frac{\partial}{\partial z} \left(K \frac{\partial N}{\partial z} \right), \quad (19a)$$

$$\frac{\partial P_i}{\partial t} = \mu_i^* P_i - \sum_j J_{pred,i,j} \frac{P_j}{x_j} - m_v P_i^2 - m_{HTL,i} P_i^2 + \frac{\partial}{\partial z} \left(K \frac{\partial P_i}{\partial z} \right), \quad (i = 1, 2, \dots, n) \quad (19b)$$

$$\frac{\partial D}{\partial t} = m_v \sum_i P_i^2 + (1 - \sigma_g) \sum_i \sum_j J_{pred,i,j} \frac{P_j}{x_j} - \sigma_g \sum_j J_{B,j} \frac{P_j}{x_j} - \gamma_r D + \frac{\partial}{\partial z} \left(K \frac{\partial D}{\partial z} \right) - w \frac{\partial D}{\partial z}. \quad (19c)$$

Here $J_{N,i}$ is the nutrient uptake by a cell of size class i . Nutrients are replenished by the excess nutrients excreted by plankton cell when carbon is limiting ($N_{E,i}$; Appendix C) and by remineralization of detritus to nutrients with rate γ_r . μ_i^* is the division rate (optimal) of cells (11 and 13). Diffusion is represented by K and detritus sink with a velocity w .

The key process is grazing by larger cells graze on smaller cells with a size preference determined by a fixed predator-prey size ratio (Equation 15) and by an increasing preference for abundant size groups (Equation 17). Further, we assume that a fraction f_B of the detritus is bacteria, such that $B = f_B D$, which are also grazed upon. The grazing rate of size class j on size class i is denoted by $J_{pred,i,j}$ (where $i = B$ represents bacteria and $i,j = 1 \dots n$ represents all plankton groups).

Besides the predation mortality, cells are exposed to mortality m_v due to viral lysis and $m_{HTL,i}$ on three largest size classes (i.e., $m_{HTL,i} = 0$ for $i = 1, \dots, 5$) due to predation by higher trophic levels. Both mortalities are proportional to the biomass to reflect that the losses increase quadratically with biomass. (This is commonly referred to as a “quadratic” mortality, though the mortality is only linear in biomass.) A fraction of the grazed material is converted to detritus because of sloppy feeding and the remaining part, σ_g , is used for growth. The same rule applies to the grazing on bacteria (detritus), and as a result, the actual reduction in detritus pool appears as σ_g , the amount used in growth.

We simulate the model up to a depth $h = 500$ m. The boundary conditions at the surface ($z = 0$) are

$$\frac{\partial}{\partial z} (N, P_i, D) \Big|_{z=0} = 0, \quad (20)$$

and at the bottom of the water column

$$\left(K \frac{\partial N}{\partial z} \right) \Big|_{z=h} = S(N_0 - N(h)), \quad (21)$$

$$\left(K \frac{\partial D}{\partial z} \right) \Big|_{z=h} = -wD(h), \quad (22)$$

$$\frac{\partial P_i}{\partial z} \Big|_{z=h} = 0. \quad (23)$$

Here z is the vertical coordinate (measured positively downward), $K(z)$ is the vertically varying turbulent eddy diffusivity, and w is the sinking speed of the detrital material. The surface boundary conditions express a zero flux through the sea surface. At the bottom of the simulated water column ($z = h$), the boundary conditions reflect an exchange of nutrients with the deep nutrient reservoir at a constant rate S (with constant nutrient concentration N_0), sinking and lost as detritus through the bottom layer to the deep water, and a zero diffusive flux of living phytoplankton.

We use the General Ocean Turbulence Model as a framework for our coupled biological-physical model (Umlauf et al., 2005) combined with the Fortran-based Framework for Aquatic Biogeochemical Models (Bruggeman & Bolding, 2014). General Ocean Turbulence Model is configured to describe the upper 500 m of the water column ($h = 500$), using 500 layers of 1 m thick. We implemented the model into six different water columns at latitudes ranging from 10°N to 60°N with 10° latitude spacing. The seasonal and latitudinal forcings are regulated by variations in seasonal surface light intensity (Figure S3 in the supporting

information), wind speed (Figure S2a), and air temperature (Figure S2b), leading to variations in water temperature (Figure S4) and turbulent diffusivity (Figure S5); see appendix D for details.

2.4. Ecosystem Structure and Function

We analyze the model results in terms of ecosystem structure: total biomass and size distribution, trophic strategies, and ecosystem functions: primary production, vertical carbon export, and energy transfer to higher trophic levels.

Trophic strategies of organisms of different size classes are diagnosed by the relative investment in phagotrophy compared to the total investment in resource uptake:

$$\phi_{TS,i}(z, t) = \frac{\phi_{F,i}^*}{\phi_{L,i}^* + \phi_{N,i}^* + \phi_{F,i}^*}. \quad (24)$$

We assume that the value of $\phi_{TS,i} < 0.2$ represents phototrophs that mainly invest in light-harvesting and nutrient uptake, while values of $\phi_{TS,i} > 0.8$ represent almost phagotrophs that mainly invest in phagotrophy, that is, “pure” zooplankton. Values of $\phi_{TS,i}$ between 0.2 and 0.8, therefore, represent different degrees of mixotrophy.

A vertical average of the mixotrophic strategy is defined by the mean $\phi_{TS,i}$ over depth and weighted by total biomass as

$$\Phi_{TS,i}(t) = \sum_z P_i(z) \phi_{TS,i}(z, t) \Delta z(z) / \sum_z P_i \Delta z(z), \quad (25)$$

where Δz is the layer thickness.

The gross primary production, Π_{GPP} ($\text{mg C m}^{-2}\text{d}^{-1}$) is calculated as

$$\Pi_{GPP} = \sum_{i,z} J_{L,i}(P_i/x_i) \Delta z(z). \quad (26)$$

In the model, only detritus can sink and transport carbon to the deep water (deeper than 500 m). The amount of carbon transported as sinking detritus ($\text{mg C m}^{-2}\text{d}^{-1}$) is

$$F_C = w_{CCN} D, \quad (27)$$

calculated at a depth of 150 m. In reality, carbon export also includes feces from higher trophic level (HTL) organisms and the total export is, therefore, higher than F_C . We expect the actual amount of organic carbon export to lie between F_C and $F_C + L_{HTL}$, where $L_{HTL} = c_{CN} \sum_{i,z} m_{HTL,i} P_i \Delta z(z)$ represents the depth-integrated loss of three largest size groups of plankton to HTLs and c_{CN} is the constant C:N Redfield ratio.

The energy transfer efficiency to the HTLs, ϵ_{HTL} , is calculated as the ratio between the carbon transferred to the HTLs through predation on the three largest size groups and the gross primary production:

$$\epsilon_{HTL} = \bar{L}_{HTL} / \bar{\Pi}_{GPP}, \quad (28)$$

where the bars represent average over time.

2.5. Data Sources for Model Comparison

Model outcomes at different latitudes from Northern Hemisphere are compared to available data sets of surface phytoplankton biomasses, depth-integrated phytoplankton biomasses, and primary productivity measured in different seasons: spring (March–May), summer (June–August), and autumn (September–November). We restrict our comparison to the Northern Hemisphere only as southern oceans are iron-limited, and we do not resolve iron in our model. Surface (7 m) phytoplankton biomass data are taken

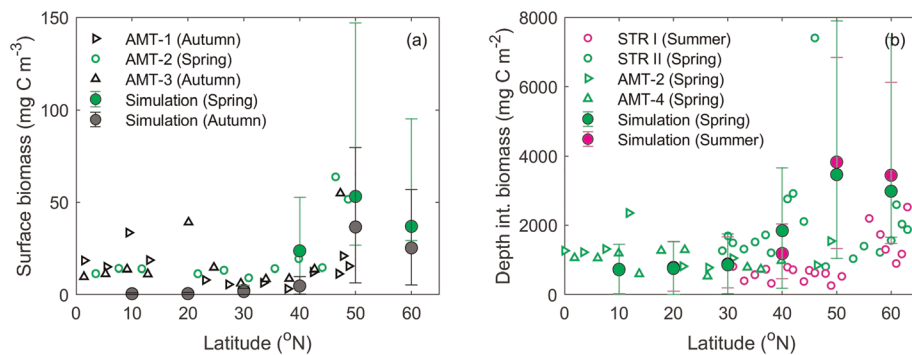


Figure 3. Comparison between observations (small open symbols) and model outcomes (large filled symbols) of surface (7 m) phytoplankton biomasses during spring (March–May) and autumn (September–November) (a) and depth-integrated phytoplankton biomasses for size range 10^{-7} to 10^{-4} µg N during spring (March–May) and summer (June–August) (b) across latitudes. Error bars represent interquartile ranges (25–75 percentile) over respective seasons. At low latitudes, simulated spring data points (green) are not visible due to overlapping with autumn data points (gray) for surface biomasses and summer data points (magenta) are not visible due to spring data points (green) for depth-integrated biomasses. For comparison, pure heterotrophs are omitted while plotting.

from three Atlantic Meridional Transect (AMT) cruises between Great Britain and the Falkland Islands taking place in 21 September–24 October 1995 (AMT-1), 22 April–22 May 1996 (AMT-2), and 16 September–25 October 1996 (AMT-3) (Marañón et al., 2000). Depth-integrated biomass data are taken from two different sources: (1) two research cruises STRATIPHYT I during July and August 2009 and STRATIPHYT II from April and May 2011 along a transect associated with a stratification gradient in the Northeast Atlantic Ocean (Mojica et al., 2015). Phytoplankton consisting of photoautotrophic prokaryotic cyanobacteria and eukaryotic algae were enumerated and size-fractionated using gravity filtration within the size range $\lesssim 20$ µm (10^{-7} to 10^{-4} µg N). Seawater samples were collected at 10 separate depths in the upper 250 m of the water column. (2) AMT-2 and AMT-4 (22 April–20 May 1997) provide depth-integrated size-fractionated chl *a* data (Marañón et al., 2001). Seawater samples were collected from 5 to 10 depths in the top 200 m of the water column and chl *a* concentrations for size group $\lesssim 20$ µm are considered for plots. Chl *a* concentrations were converted to carbon biomass using the value 40 mg C (mg chl *a*)⁻¹ (Jakobsen & Markager, 2016). During all cruises, both cell counts and chl *a* concentrations were measured. To compare empirical phytoplankton data and the model outcome, we use the approximate measure of the total biomass in the size range 10^{-7} – 10^{-4} µg N by neglecting heterotrophs ($\phi_{TS,i} > 0.8$) and convert simulated autotroph and mixotroph biomasses from nitrogen to carbon units using the Redfield ratio c_{CN} . Each of these measures represents different aspects of plankton biomass (total biomass of cells in a size range and total photosynthetically active biomass).

Primary production data are collected from two different sources: (1) two cruises in the North Atlantic Ocean between the Canary Islands and Iceland in July–August 2009 and April–May 2011 (van de Poll et al., 2013). For the measurement of primary production, five groups were chosen: group 1: Prochlorococcus; group 2: Synechococcus; group 3: Prasinophyceae, Pelagophyceae, and Cryptophyceae; group 4: Haptophyceae and Dinophyceae; and group 5: diatoms, and the productivities were measured according to Platt et al. (1980) for a 24 hr period over 1 hr time intervals in the euphotic zone (0.1% PAR). (2) AMT-1, AMT-2, AMT-3, and AMT-4 cruises between Great Britain and the Falkland Islands (Marañón et al., 2000, 2001). The rates of inorganic carbon fixation were determined at 5–7 depths by using simulated in situ incubations with the radioisotope ¹⁴C.

The predicted relative contributions to primary productivity by three major size classes (microplankton, nanoplankton, and picoplankton) are also compared with modeled satellite data that distinguishes the three major size classes from Sea-viewing Wide Field-of-view Sensor ocean color measurements over a 10-year period from 1998 to 2007 (Uitz et al., 2010). For comparison, we classify size classes 10^{-7} – 10^{-6} µg N as picoplankton, size classes 10^{-5} – 10^{-4} µg N as nanoplankton, size classes 10^{-3} – 10^{-2} µg N as microplankton, and size classes 10^{-1} –1 µg N as mesoplankton.

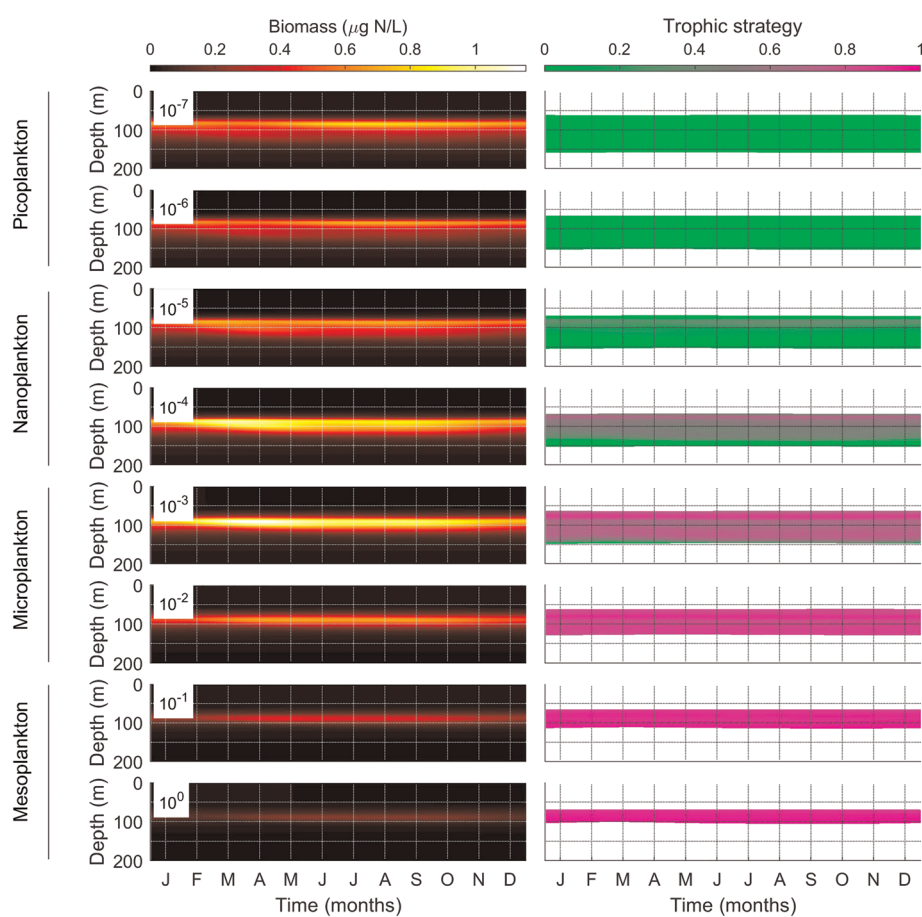


Figure 4. Biomasses of organisms of different size classes (in $\mu\text{g N}$; first column) and their trophic strategies, ϕ_{TS} , (second column) in the top 200 m at 10°N . Size increases from top to bottom. For trophic strategy, green represents phototrophs, magenta represents heterotrophs, and colors in between represent different degrees of mixotrophy. Trophic strategies are plotted only when the biomass is $>5\%$ of the maximum biomass of all size classes over the whole time period.

3. Results

3.1. Unicellular Plankton Biomasses Across Latitudes

Observations of surface (phyto)plankton biomasses and depth-integrated biomasses show a clear latitudinal variation (Figure 3, open symbols). The model displays low biomasses at low latitudes with a transition to high biomass between 40°N and 50°N . A similar pattern is seen in the data, though with a smaller difference in biomass between low and high latitudes. Relatively higher surface biomasses at low latitudes ($10\text{--}20^\circ\text{N}$) in the data compared to the model outcome result from advective transport of nutrients to the surface waters (Oschlies, 2002) which is not included in the model (Figure 3a). Above 50° the model predicts a slight dip in both biomasses, which is not evident in the summer depth-integrated biomass data (Figure 3b). At low latitudes ($10\text{--}30^\circ\text{N}$), the total plankton biomass does not exhibit significant seasonal variation, whereas above 30°N , seasonal variability is evident. It is harder to see the seasonal variation in the data due to a paucity of observations. Overall, however, the general level of biomasses is similar between model outcome and observations.

3.2. Community Composition and Trophic Strategies

Our model predicts a significant difference in the seasonal community compositions (both size distributions and trophic strategies) between 10°N and 60°N (Figures 4 and 5). Low latitude waters typically show a subsurface biomass maximum throughout the year (Figure 4) with the coexistence of all size groups. Picoplankton, nanoplankton, and microplankton show similar contributions (~30%) to the total biomass,

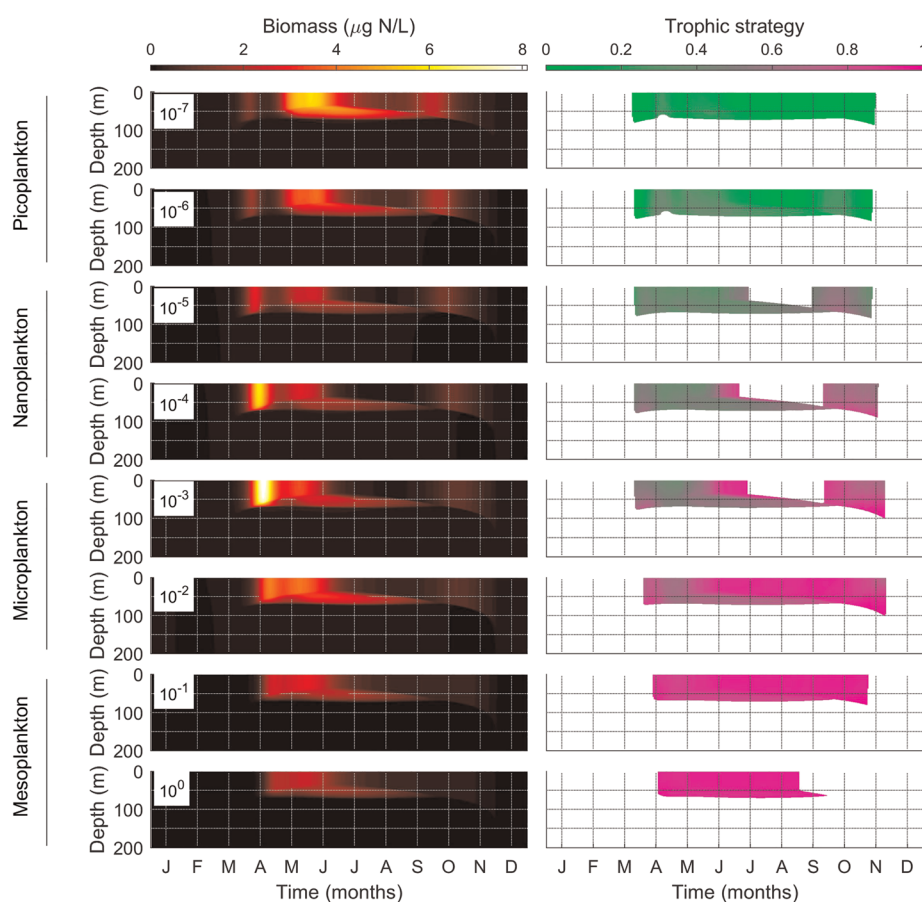


Figure 5. As Figure 3 but at 60°N.

whereas the contribution from mesoplankton remains consistently low (~10%) throughout the year (Figure 6a). The emergent trophic strategy, ϕ_{TS} , varies systematically with size and depth: Picoplankton are mainly phototrophic. Mixotrophy is the dominant strategy for nanoplankton and small microplankton but only in the upper part of the water column; they invest more in light as light becomes limiting with increasing depth and adopt more phototrophic strategy (second column of Figure 4). In spite of being cheaper, investment in phagotrophy does not provide any significant benefit to the organisms because of negligible food biomass in deep water. Consequently, organisms increase their investment in relatively expensive phototrophy to obtain carbon (Berge et al., 2017). Similar high investment in light-harvesting apparatus in light-limited deep water was previously simulated by Bruggeman and Kooijman (2007) and Clark et al. (2013). Large microplankton and mesoplankton appear as pure heterotrophs independent of depth and season.

In contrast, at 60°N, a clear seasonal succession of trophic strategies of different sized cells is observed (Figure 5). The optimal trophic strategy can be interpreted as a change in the community composition (different populations or taxa). During winter, plankton biomasses are very low due to the combination of low light and a deep mixed layer. With the onset of stratification in April, all plankton size classes with phototrophic ability start to increase. However, the nutrients are not yet depleted, and therefore, nanoplankton and microplankton dominate the surface mixed layer by outcompeting picoplankton. Although these large nanoplankton and microplankton appear as mixotrophs in the model, their growth mainly depends on phototrophic pathway as the gain from phagotrophy is negligible compared to gain from phototrophy (Figure S8). In late May, a shift in the community composition from the dominance of nanoplankton and microplankton to the dominance of picoplankton in the surface mixed layer (~35%–40% of the total biomass) is simulated (Figures 5 and 6b). This shift is associated with the increase in biomasses of large heterotrophs

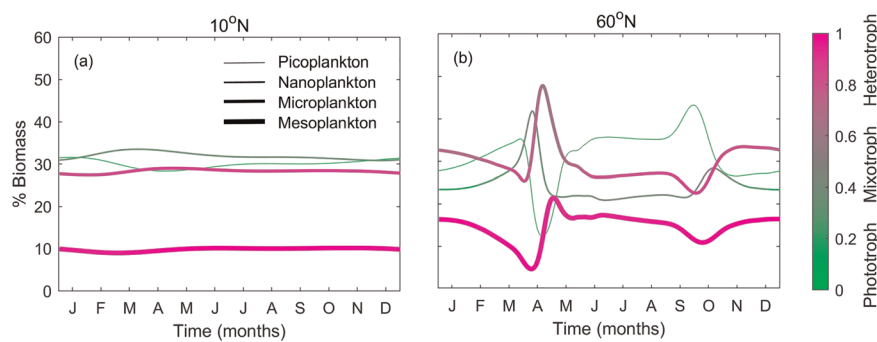


Figure 6. Monthly average of relative contributions in biomasses by different size groups of plankton (line widths) and trophic strategies (line color). At 10°N (a) and 60°N (b).

that exert grazing pressure on nanoplankton and microplankton in combination with a reduction in nutrient concentration. During summer (June–August), nutrients are depleted in the surface water and phototrophic picoplankton remain the dominant group. Although one can expect that under nutrient limiting summer conditions, mixotrophy and heterotrophy should be the dominant strategies (Chakraborty et al., 2017), but low nutrient areas are associated with very low biomasses in our simulation, and as a result, phagotrophy is not advantageous in these areas. However, subsurface biomass maximum during summer dominated by picoplanktonic cells, with both phototrophic and mixotrophic strategies, is observed (Figure 6b). Similar high summer surface picoeukaryote dominance was observed in observations (Mojica et al., 2015).

The emergence of different trophic strategies during the succession are shown in (Figures 7 and S11). All biomasses are pooled and plotted according to their strategy. The dominant axis from top left to bottom right represents the heterotroph (top left) to phototroph (bottom right) continuum. Overall, both extreme strategies emerge clearly (Figure 7a), but the entire continuum is populated. Differences are clear during the succession with mixotrophs (around the center) very abundant in spring (Figure 7b), coexistence of the entire continuum during summer (Figure 7c), and dominance of either phototrophs or heterotrophs during autumn (Figure 7d). The axis from the center toward origin represents the investment in nutrients (marked by the arrow in Figure 7a). Generally, investments in nutrients are small because they are relatively inexpensive. Exceptions are clear during summer (Figure 7c) and in the surface (Figure 7e) where nutrients are depleted.

3.3. Variations in the Mixotrophic Size Range With Latitude

The trophic strategy of organisms varies with latitude (Figure 8). Although the mixotrophic size range almost remains the same at low latitudes irrespective of the season, high latitudes show variability in terms of both the size of mixotrophic cells as well as the size range of organisms with mixotrophic strategy. At high latitudes, mixotrophy appears as a suitable strategy and dominates among small picoplanktonic size classes in the deep chlorophyll/subsurface maximum during summer (Figures 5 and 8b). On the other hand, early spring conditions favor large mixotrophs in the surface mixed layer and the mixotrophic behavior is restricted to a narrower range of cell sizes (Figures 5 and 8a).

3.4. Ecosystem Functions: Primary Productivity, Vertical Transport of Carbon, and Energy Transfer to HTLs

3.4.1. Primary Productivity

Patterns of depth-integrated primary productivity are in fair agreement with field data across latitudes (Figure 9). Although field data are relatively sparse at low latitudes (10–30°N) without showing any specific trend of spring primary productivity, model outcome shows low primary productivity ($\sim 100 \text{ mg C m}^{-2} \text{ day}^{-1}$) with almost no seasonal variability (Figures 9a and 9b). The primary productivity is dominated by picoplankton and nanoplankton with equal contribution of ~40%–45% each throughout the year (Figure 10a). In spite of having ~30% relative contribution in biomass production (Figure 5a), microplankton contributes relatively less to productivity (~15%). This is not due to metabolic scaling, but due to high investment in phagotrophy, it reflects the heterotrophic nature of microplankton at low latitudes. In contrast, a larger seasonal variability of

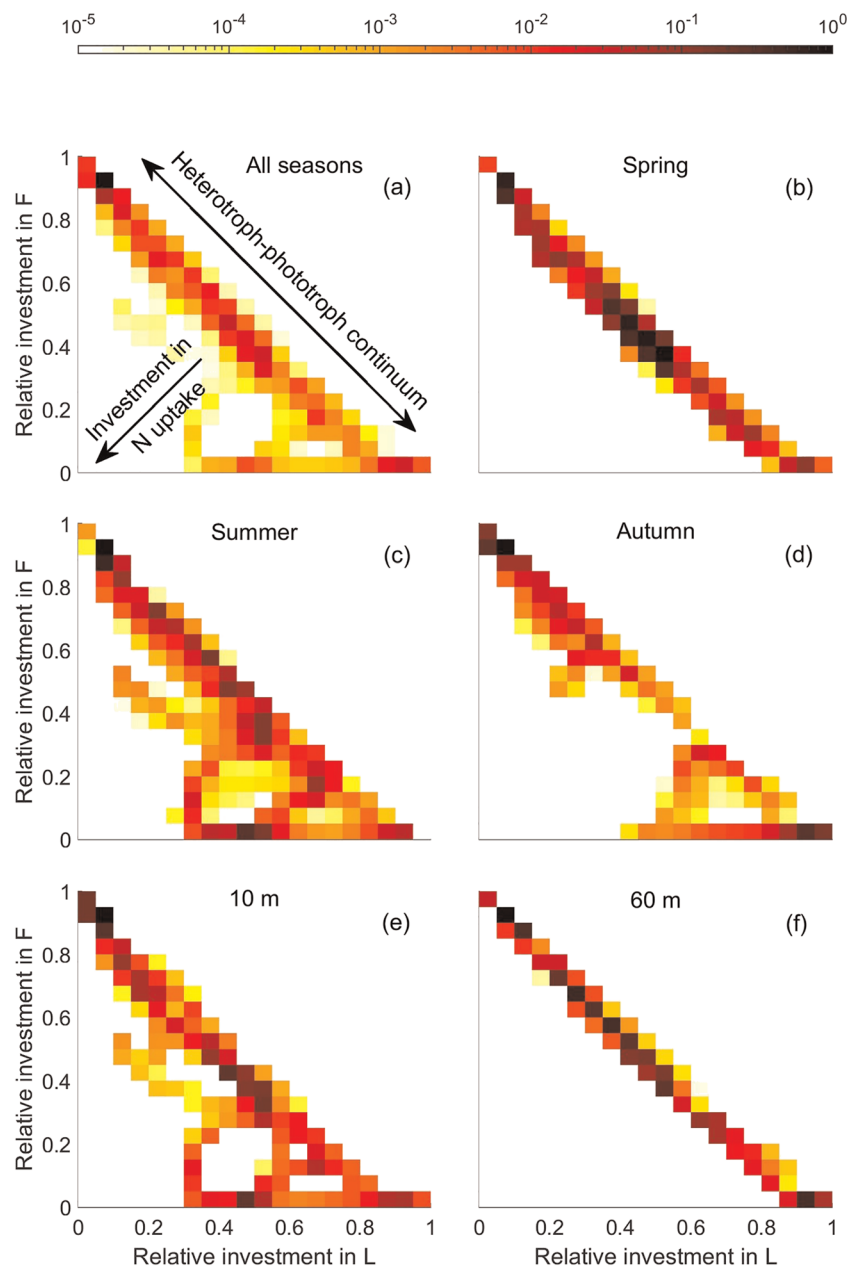


Figure 7. Density of strategies for average over depth and all seasons (a), spring (b), summer (c), autumn (d), average over all seasons at 10 m (e), and 60 m (f) at 60°N with respect to relative investments in phototrophy and phagotrophy. The densities are calculated as 2-D histograms (in relative investments, $\phi_{TS,i}$, in L and F) multiplied by biomass and normalized by the maximum for each case.

primary productivity is observed in both model and data at high latitudes (50 and 60°N) with a significant increase during spring and early summer (Figures 9a and 9b). This spatiotemporal pattern shift between 40° and 50° reflects year-round stratification at lower latitudes and the increased production results from when the mixed layer is broken down during winter, which happens somewhere between 40° and 50° (Figure S5). The increased production is therefore mainly driven by physics, and differences in mixing patterns between model and observations are probably responsible for the differences between modeled and observed production at 40°N. Primary productivity is relatively low during autumn peak, showing the inclination towards heterotrophic nature of the unicellular plankton community in autumn compared to the autotrophic strategies during spring. Consistent with the relative contributions to biomass, the high

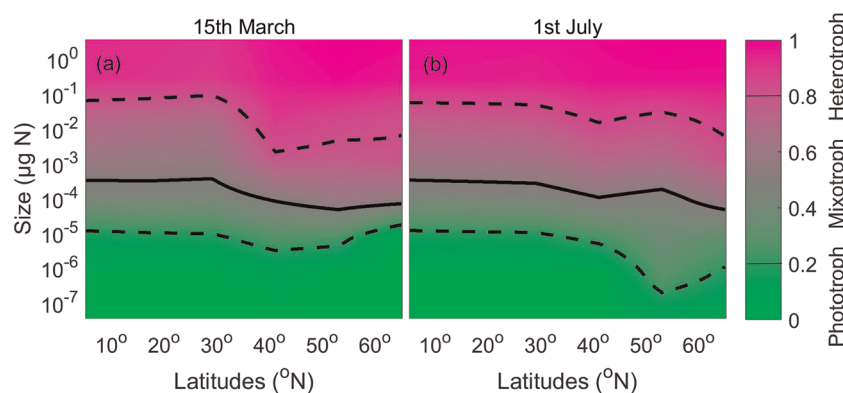


Figure 8. Mixotrophic size range at different latitudes on 15 March (a) and 1 July (b). The solid lines show the trophic strategy $\phi_{\text{TS}} = 0.5$, and the dashed lines show $\phi_{\text{TS}} = 0.2$ and 0.8 (Equation 14).

spring primary productivity results from the high relative contribution by nanoplankton and microplankton, whereas picoplankton are responsible for summer primary productivity (Figure 10b). The contribution in primary production by mesoplankton remains consistently low irrespective of season and latitude. The overall relative contribution by three groups (picoplankton, nanoplankton, and microplankton) fits well with the empirical model outcomes of Uitz et al. (2010). They found microphytoplankton as the major contributor to the total primary production in temperate regions (~50%) during the spring, while nanophytoplankton provides continuous substantial contribution (40%–60%) irrespective of latitudinal and seasonal variation.

3.4.2. Vertical Transport of Carbon

The vertical carbon export shows increasing trends with latitude with higher variability at high latitudes (Figure 11). Carbon export remains consistently low throughout the year at low latitudes ($<40^{\circ}\text{N}$) whereas clear seasonal variabilities can be observed at high latitudes. The maximum possible carbon export does not change much over the year at lower latitudes compared to higher latitudes, but the detrital export shows slightly higher relative export fluxes during summer. Such consistent low maximum possible carbon export is due to low HTL export at lower latitudes. The maximum export occurs during the end of the spring bloom at higher latitudes. Interestingly, the pattern of detrital export at 40° is different from everything else and peaks during the transition of winter and spring.

3.4.3. Energy Transfer Efficiency to HTLs

The annual average energy transfer efficiency increases with latitude (Figure 12). The differences in biomasses of microplankton and their trophic strategies at different latitudes are responsible for the differences in transfer efficiencies. On one hand, we have considered quadratic predation term on the three largest size

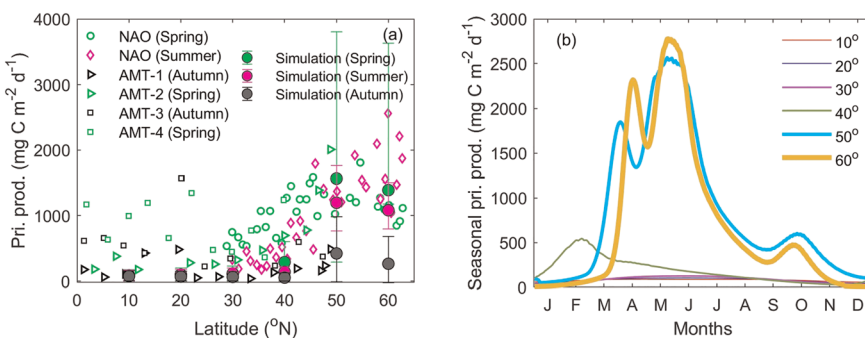


Figure 9. Depth integrated gross primary productivity across latitudes at different seasons (a) and model outcome of seasonal primary productivity at different latitudes (b). Small open symbols represent data from different cruises (see text) whereas large filled symbols are model outcome. Error bars represent interquartile ranges (25–75 percentile) over respective seasons. At low latitudes, simulated spring (green) and summer data points (magenta) are behind the autumn data points (gray).

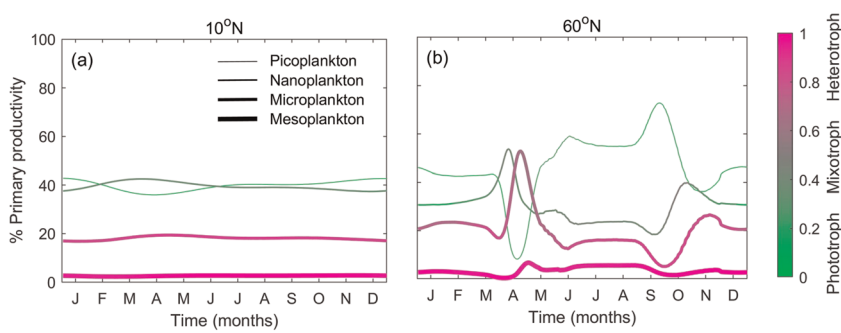


Figure 10. Monthly average of relative contributions in primary productivity by different size groups (line widths) of plankton at 10°N (a) and 60°N (b) together with their trophic strategies (line color).

groups by HTLs, and as a result, high biomasses at high latitudes are efficiently transferred to HTLs than the relatively lower biomasses at low latitudes. On the other hand, microplankton invest more in phototrophy during spring at high latitudes and it helps to increase transfer efficiency.

3.5. Sensitivity Analysis

The sensitivity of the model outcome is examined by varying some of the parameters by $\pm 50\%$ from their default values (Table 1). Specifically, we check the sensitivity of depth-integrated biomasses, depth-integrated primary productivities, estimation of total carbon export, energy transfer efficiency, and the size range of mixotrophs at different latitudes by varying affinities for resources (α_L , α_N , α_F), resource uptake costs (β_L , β_N , β_F), and predation by higher trophic levels m_{HTL_8} . For the sensitivity test, we use the sensitivity index (I) as $I = (\bar{X}_p - X_p) \times 100/X_p$, where X_p is the value of the variable with reference parameters mentioned in Table 1 and \bar{X}_p is the value of the variable obtained when the parameter is varied by $\pm 50\%$. This measure gives the relative change of the variable with respect to changes in parameters (supporting information Figures S12–S15). Low and high latitude spring biomasses are sensitive to α_L and α_F ; maximum biomass decrease occurs due to the decrease in α_L whereas maximum biomass increase results due to a decrease in α_F . On the other hand decrease in α_L and α_F result in maximum decrease and increase in low latitude summer biomasses, respectively, whereas the decrease in β_F and m_{HTL_8} result in maximum decrease and increase in high latitude summer biomasses, respectively. Although the sensitivity of low latitude primary productivity does not depend on the season and show similar changes as α_L change, high latitude summer and autumn primary productivity show maximum changes with β_F whereas, maximum decrease and increase of high latitude spring primary productivity result from the decrease in α_L and α_F . α_L remains one of the sensitive parameters for detritus sinking and maximum possible limit of carbon export through the depth 150 m at low latitude together with m_{HTL_8} . m_{HTL_8} also determines changes in maximum carbon export at high latitude whereas maximum decrease and increase of detritus sinking occur with

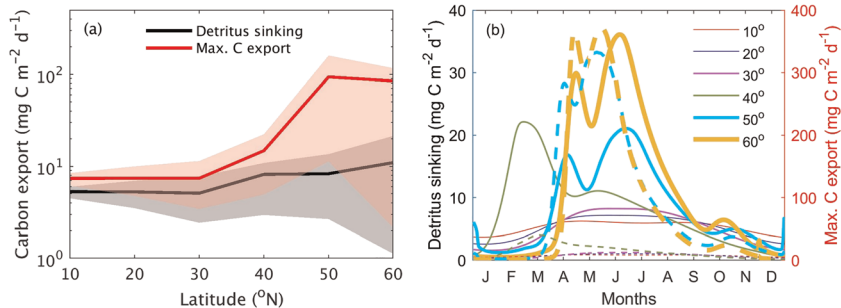


Figure 11. (a) The range of annual average carbon export that lies within detritus export (black) and maximum possible carbon export (detritus + HTL export) (red) at depth 150 m across latitudes. Shaded regions represent the interquartile range (25–75 percentile). (b) Seasonal variation of detritus export (continuous line; left y axis) and maximum possible carbon export (dashed line; right y axis) at depth 150 m at different latitudes.

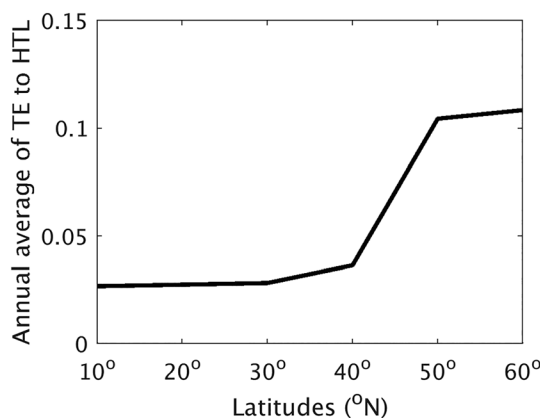


Figure 12. Annual average transfer efficiency (ϵ_{HTL}) to the higher trophic levels as a function of latitude.

decrease in α_L and α_F , respectively. Increase in annual average energy transfer efficiency mainly results from the decrease in β_F whereas its decrease is sensitive to α_L , α_F and m_{HTL} . Mixotrophic size range becomes narrower and mixotrophy appears as limited to only relatively larger organisms with an increase in α_L , whereas an increase in α_F shows a completely opposite trend.

4. Discussion

The model predicts how variation in the seasonal forcing, mainly, the variation in the amplitude of light, shapes the structure, and function of the unicellular pelagic ecosystem. In general, two regimes can be discerned: low latitude tropical systems with low biomass and higher latitude system with high biomass. The driving force is whether the cooling in the winter season and the increased wind forcing is strong enough to break up the stable stratification and bring nutrients up into the photic zone. This transition is well known, and the model generally predicts the increase in bio-

mass levels with latitude. The transition also brings about changes in the trophic structure with low latitudes having larger mixotrophs. The transition to a seasonally broken stratification does not bring much increase in the detritus sinking flux in the model; however, due to increased transfer of energy to higher trophic levels, there is a large increase in the detrital flux from higher trophic levels (copepods and fish). Overall, the direct physical forcing on the water column is sufficient to drive these latitudinal changes in the structure and function of the simulated ecosystem, even without the representation of temperature on the physiology of the plankton.

The model of the unicellular plankton ecosystem reproduces general observed patterns of latitudinal variation in community structure and ecosystem functions. Trophic strategies are emergent outcomes and not prescribed by the model setup; the degree to which cells are autotrophic or heterotrophic depends on the environment and varies over time and space. The model is based on very few fundamental assumptions: Big cells eat smaller cells, the trade-offs associated with investments in three resource harvesting traits, and how resource uptakes are limited by cell size. These assumptions can be viewed as universal in the sense that they are ultimately determined by laws of physics or by physiological limitations. This mechanistic basis means that there is no regional-specific tuning and the model is therefore suitable for inclusion in large scale circulation models, for instance, to explore the global impact climate change.

The model implements the instantaneous adaptation (Smith et al., 2016) to be valid not only for nutrient uptake traits but for the entire plankton community model from phytoplankton to zooplankton. Most current models of plankton communities are based on plankton functional types (PFTs). PFTs can represent specific taxonomic groups, such as diatoms and flagellates, or may be linked to specific traits such as size (e.g., ERSEM, and MEDUSA; Butenschön et al., 2016; Yool et al., 2013). In either case, the parameters in the PFTs represent the average of the species in each group, typically dominated by a few species. By tuning the parameters, PFT-based models have the flexibility to be accurately calibrated to a regional-specific plankton community. However, because the parameters are fixed, the models lack the ability to represent changes in the community. This may not be a concern for regional simulations, for which parameters are fairly constant, but for global-scale simulations, PFT models may struggle to reproduce real-world variation in processes and interactions. Recent model development overcomes some of these issues by accounting for a large number of potentially viable phytoplankton types with parameter values determined by observed relations (e.g. Follows et al., 2007; Ward et al., 2012). However, these models still distinguish between functional groups of phytoplankton and zooplankton and, thereby, do not account well for mixotrophy. The first global model to completely forgo the phytoplankton/zooplankton classification is the purely size-based model of Ward and Follows (2016). Alternatively, mixotrophy has been resolved explicitly as a trait by Bruggeman (2009). That model, however, only considered one trophic level. The present model avoids a priori distinction between functional types, instead allowing functions to emerge as a consequence of a few essential key traits (size and investments into different resource harvesting strategies). Different trophic strategies are an emergent outcome as a function of the environment. As a result, the model captures

Table 1
Central Symbols and General Parameters

Symbol	Definition	Value and unit
L	Light flux in the environment	W m^{-2}
N	Concentration of nutrients in the environment	$\mu\text{g N/L}$
F	Concentration of food in the environment	$\mu\text{g N/L}$
$A_{L,i}$	Affinity for light. Value determined by traits	$\mu\text{g C}/(\text{W m}^{-2}\text{day})/\#$
$A_{N,i}$	Affinity for nutrients. Value determined by traits	$\text{L/day}/\#$
$A_{F,i}$	Affinity for food. Value determined by traits	$\text{L/day}/\#$
$J_{X,i}$	Flux of assimilated substance or respiration	$\mu\text{g C/day}/\# \text{ or } \mu\text{g N/day}/\#$
$\phi_{X,i}$	Investment traits	Variable ($\mu\text{g N}/\mu\text{g N}$)
x_i	Total mass of the cell	Variable ($\mu\text{g N}/\#$)
$m_{m,i}$	Mass of cell membrane	Calculated ($\mu\text{g N}/\#$)
α_L	Affinity per investment in light	1.36 $\mu\text{g C}/(\text{W m}^{-2}\text{day } \mu\text{g N})$
α_N	Affinity per investment for nutrients	0.568 $\text{L}/(\text{day } \mu\text{g N})$
α_F	Affinity per investment for food	0.3408 $\text{L}/(\text{day } \mu\text{g N})$
c_L	Parameter that determines how the maximum photosynthetic affinity scales with size	0.0923 $\mu\text{g C}/(\text{W m}^{-2}\text{day } \mu\text{g N}^{2/3})$
c_N	Parameter that determines how the maximum nutrient affinity scales with size	$2.8904 \times 10^{-4} \text{ L}/(\text{day } \mu\text{g N}^{1/3})$
c_F	Parameter that determines how the maximum food affinity scales with size	0.2272 $\text{L}/(\text{day } \mu\text{g N})$
M_L	Max. uptake rate per investment for light	17.04 $\mu\text{g C}/(\text{day } \mu\text{g N})$
M_N	Max. uptake rate per investment for nutrients	6.816 day^{-1}
M_F	Max. uptake rate per investment for food	5 day^{-1}
β_L	Cost of photosynthesis	
β_N	Cost of nutrient uptake	0.08 $\mu\text{g C}/\mu\text{g C}$
β_F	Cost of food uptake	0.4544 $\mu\text{g C}/\mu\text{g N}$
r_0	Cost of maintenance of structure	0.4544 $\mu\text{g C}/\mu\text{g N}$
r_L	Cost of maintenance of chloroplast	0.2272 # $\mu\text{g C}/(\mu\text{g N day})$
r_N	Cost of maintenance of nutrient uptake organelles	1.0224 # $\mu\text{g C}/(\mu\text{g N day})$
r_F	Cost of maintenance of phagotrophic organelles	0.2272 # $\mu\text{g C}/(\mu\text{g N day})$
β	Preferred predator-prey mass ratio	1,000
σ	Niche width	1
γ_g	Fraction of grazing devoted to growth	0.7
γ_r	Regeneration rate of nutrient from detritus pool	0.1 day^{-1}
m_v	Mortality due to viral lysis including natural mortality	0.03 $\text{L}/(\text{day } \mu\text{g N})$
$m_{\text{HTL}, i}(i = 1 - 5)$	HTL predation rate on size classes	0.0 day $^{-1}$
$m_{\text{HTL}, 6}$	HTL predation rate on size class 6	$m_{\text{HTL}, 8}/2 \text{ day}^{-1}$
$m_{\text{HTL}, 7}$	HTL predation rate on size class 7	$m_{\text{HTL}, 8}/1.2 \text{ day}^{-1}$
$m_{\text{HTL}, 8}$	HTL predation rate on size class 8	0.07 day^{-1}
S	Diffusive exchange rate between bottom layer and deep water	0.2 day^{-1}
N_0	Nutrient concentration in the bottom	280 $\mu\text{g N/L}$
w	Sinking rate of detritus	5 m day^{-1}
f_B	Fraction of detritus biomass converted into bacterial biomass	0.1
ϕ_L	Investment in the photosynthetic machinery	—
ϕ_N	Investment in nitrate harvest	—
ϕ_F	Investment in phagotrophy	—
c_{CN}	C/N ratio in food and in the cell	5.68 $\mu\text{g C}/\mu\text{g N}$

Note. Index X refers to light (L) measured in units of W m^{-2} , nutrients (N) in units of $\mu\text{g N/L}$, or food (F) in units of $\mu\text{g N/L}$. Units of “1/#” represent “per cell” and “L” refers to liters.

emergent trophic strategies of unicellular plankton of different size classes, and how it differs across latitudes.

4.1. Optimization Procedure

The model employs an optimization framework to reduce the number of state variables and computational effort. A similar instantaneous optimization approach was previously applied in a dynamic phytoplankton model where individuals are allowed to maximize their growth rate by regulating their intracellular resource allocation in carbon versus nitrogen assimilation and affinity for nutrient versus maximum uptake rate (Smith et al., 2016). In the present study, optimization implicitly assumes that the entire community adapts its trophic strategy plastically and instantaneously. In reality, some aspects of adaption do indeed happen fast. Photoacclimation, for example, whereby cells adjust their investment in chloroplast according to

light conditions, occurs on a time scales of hours (Masojídek et al., 1999), which in a global simulation would appear as instantaneous. However, adaptation in investments in nutrient uptake or phagotrophy is likely less adaptable. Changes in these traits in nature would mainly occur through demographic changes, where species with traits close to the current optimal trait combination outcompete those with less optimal traits. Steady state multispecies competition experiments show that such species replacements take place in a time frame of 2–4 weeks (Smith & Kalff, 1983; Sommer, 1983). In periods of rapid change, such as a spring bloom situation, the model with instant optimization will therefore adapt itself faster than a real community would be able to. Fully resolving this adaption requires a dynamic description of all possible trait combinations, which is computationally very expensive. A computationally more attractive approach is moment closure techniques that only resolve the first or second moments of the trait distribution (Bruggeman & Kooijman, 2007; Norberg et al., 2001; Wirtz & Eckhardt, 1996). Such moment-closure models have shown that periods, where the optimum is out of phase with the community, are rare (Terseleer et al., 2014), giving some confidence in the optimization approach pursued here. Further, we see that the model is able to resolve the seasonal succession in production and carbon loss even without resolving the out of phase situations.

4.2. Variations in Optimal Trophic Strategies

Organisms mostly invest in photosynthesis in light-limited nutrient-replete deep waters whereas nutrient-deplete high latitude summer waters show high relative investment in nutrient uptake. Such variation can also be observed among organisms of different size classes. As small phototrophs suffer relatively less from nutrient limitation, they mainly invest in photosynthesis; the relative investment in nutrient uptake increases with the size of phototrophic organisms. On the other hand, mixotrophy is mainly limited within nanoplankton and microplankton groups in low latitudes, whereas the dominance of small bacterivorous mixotrophic picoplankton can also be observed at high latitude waters during the end of spring and autumn (Sanders & Gast, 2012). The availability of bacterial prey and sufficient light during this time of the year provide mixotrophs an advantage against pure phototrophs and make mixotrophy a suitable strategy among picoplankton. In the absence of diatoms, large mixotrophs dominate high latitude waters during spring (Lavrentyev & Franzè, 2017). The combination of high nutrients and prey makes mixotrophy favorable against pure phototrophs and phagotrophs.

Although the model does not distinguish between different pathways of acquiring chloroplast by mixotrophs, it essentially captures the essence of all of the strategies. For example, constitutive mixotrophs have their own chloroplasts to perform photosynthesis and are relatively smaller. In comparison, non-constitutive mixotrophs obtain their chloroplasts from phototrophic prey to use in photosynthesis until they degrade and tend to be relatively bigger and more heterotrophic in nature. Our model mimics the existence of both, small and large mixotrophs with their inclinations toward phototrophy and phagotrophy, respectively.

4.3. Prospectus

In this work, we have confined ourselves to resolve the unicellular component of the marine ecosystem using only the traits of cell size and investment in resource uptakes. Confining the model to these four traits essentially assumes that all organisms are naked mixotrophs, similar to flagellates or dinoflagellates. However, the diversity of unicellular organisms involves some important specializations, in particular diatoms and diazotrophs.

Diatoms are the dominant component during spring bloom in high latitudes (Hutchinson, 1941; Smetacek, 1999) and in upwelling areas in lower latitudes (Taylor & Landry, 2018). Diatoms differ from the cells in the present model by being purely autotrophic and by having a vacuole whereby their physical size increases to provide a benefit in terms of increased nutrient uptake and photosynthesis and decreased predation. The closest the model comes to representing a diatom strategy is the relatively large cells (10^{-4} – 10^{-2} µg N) occurring in significant biomasses during spring at high latitudes. However, despite obtaining little benefit from phagotrophy, these cells still invest a significant amount in phagotrophy in our model. This is because investing in phagotrophy appears cheaper than investing in two other traits that would incur more costs than benefits. The model could in principle be extended with traits representing vacuole formation and developing a silica frustule, together with related trade-offs in terms of extra metabolic costs and silica dependence, and benefits from resource acquisition, reduction in predation pressure, and buoyancy regulation (Hansen & Visser, 2019). We expect that these traits would provide more benefit

than phagotrophy during spring at high latitudes and allow big vacuolated cells covered with silica frustule (diatoms) to dominate during spring in high latitudes (Cadier et al., 2019). Another missing strategy is diazotrophy, that is, N₂ fixation. Similar to vacuole and silica shell, nitrogen fixation could be incorporated as an additional trait in the present framework. The main trade-offs would then be the direct energetic cost of N₂ fixation together with a reliance on available iron (Kustka et al., 2002) and the very high cost of managing intracellular oxygen (Großkopf & LaRoche, 2012), which precludes the possibility of diazotrophs to invest into phagotrophy. Indeed, the mutual exclusivity of phagotrophy, diazotrophy, and shell formation is a feature that can be exploited to simplify the full trait-based description of unicellular planktonic life into three parallel, competing functional groups for mixotrophs (as illustrated here), diatoms, and diazotrophs.

An additional limitation of the current version of the model is the absence of temperature regulation on key physiological processes within the cell and on ecological interactions. Temperature is known to affect metabolic processes by regulating enzymatic activities (Raven & Geider, 1988) and affect nutrient uptake by temperature-dependent diffusion (Thingstad & Aksnes, 2019), while phototrophy is relatively unaffected by temperature (e.g., Blackman, 1905). At the environmental level, increased temperature tends to limit nutrient availability via stratification and decreased mixing, however, that aspect is well resolved by the model. Therefore, the overall effect of temperature depends on a complex interplay between these physiological and environmental processes. Recent theory and meta-analysis predict a stronger temperature dependence of heterotrophic metabolism compared to autotrophic metabolism (Allen et al., 2005; López-Urrutia et al., 2006; Rose & Caron, 2007) that can result in an increase in heterotrophic nature of mixotrophs with rising temperature (Wilken et al., 2013). The mechanistic formulation of the model makes it well suited by incorporation of such well-known temperature dependencies of each mechanism (Serra-Pompei et al., 2019). The overall temperature response of the investment and the community is therefore complex and hard to predict without the model (Serra-Pompei et al., 2019). For example, with high prey availability, we expect higher investments in phagotrophy than phototrophy, because it is a cheaper investment. Conversely, in low prey environments increasing temperatures may result in higher investments in phototrophy.

Finally, in order to more properly address the biogeochemical cycles of the ocean, the model needs better representation of detrital dynamics—the production and sinking of particulate matter, its remineralization, repackaging and changing stoichiometry (Sanders et al., 2014), and the active transport by vertically migrating zooplankton (Steinberg & Landry, 2017) and mesopelagic fish (St. John et al., 2016). By resolving the size spectrum of productivity, the current model comes a long way in resolving processes in the production and sinking of detrital material (Boyd & Newton, 1999). This would be further advanced with a “diatom” functional group to account for their central role in the vertical flux of carbon and nutrients (Kemp et al., 2000; Smetacek, 1999; Tréguer & De La Rocha, 2013). In a similar manner, the active vertical transport of carbon has been shown to be accessible to a trait-based approach (Hansen & Visser, 2016) and used to map shifts in carbon sequestration in the North Atlantic (Brun et al., 2019). All of these features are accessible through the same conceptual modeling framework outlined here, providing an integrated platform spanning from primary production to marine ecosystem services such as carbon sequestration and fisheries production.

5. Conclusion

We have developed a generic multitrophic, multitrait framework to model unicellular plankton communities. The model is economic in state variables and number of parameters, yet it captures the adaptability and diversity of plankton organisms by instantly optimized traits. Despite its conceptual simplicity, the model represents the latitudinal variation in plankton structure and function. The emergent correlations between plankton traits and cell size highlight the importance of cell size to determine the ability and function of individual cells. Each size group in the plankton, therefore, plays a different role in the function of the entire community. However, the role is not fixed; the community within a size group changes according to the environmental conditions. A full representation of the plankton community, either in a model or as observations, therefore, requires combining cell size with other traits. These traits can either be a continuous representation of function, as done here, or by discrete functional groups. These features make the model well suited for global-scale simulations under environmental change.

Appendix A: Calculation of the Fraction of Mass Devoted to Organelles

To calculate the mass of the membranes, we follow the procedure of Clark et al. (2013) and assume that the cell is perfectly spherical with radius r_i . Total membrane volume consists of two parts: outer membrane and cytoplasmic membrane (thickness t_{om} and t_{cm}) with periplasm (thickness t_p) within the two membranes. The total membrane volume ($V_{\text{m},i}$ μm^3) is

$$V_{\text{m},i} = \frac{4\pi}{3} \left[(r_i^3 - (r_i - t_{\text{om}})^3) + ((r_i - t_{\text{om}} - t_p)^3 - (r_i - t_{\text{om}} - t_p - t_{\text{cm}})^3) \right] \quad (\text{A1})$$

The corresponding total mass of the cellular membrane can be calculated as

$$m_{\text{m},i} = V_{\text{m},i} \rho_m c_{\text{CN}}^{-1}, \quad (\text{A2})$$

where ρ_m ($\mu\text{g } \mu\text{m}^{-3}$) is the membrane density.

The total dry mass (x_i) of the cell of radius (r_i) is

$$x_i = \frac{4\pi}{3} r_i^3 \rho_{\text{cell}} g_{\text{dw}} c_{\text{CN}}^{-1}, \quad (\text{A3})$$

where g_{dw} (g g^{-1}) is the dry weight to wet weight ratio of the cell and ρ_{cell} ($\mu\text{g } \mu\text{m}^{-3}$) is the overall cell density.

Therefore, the fraction, $\phi_m(x_i)$, of cell mass of the size class i occupied by cell membranes can be written as $m_{\text{m},i}/x_i$.

By varying r_i , we get the relationship between total mass (x_i) and relative investments ($\phi_{\text{L},i} + \phi_{\text{N},i} + \phi_{\text{F},i}$) (from Equation 1) which increases with total mass (Figure A1). The parameter values used $t_{\text{om}} = t_{\text{cm}} = 8 \times 10^{-3}$ μm (Clark et al., 2013), $t_p = 15 \times 10^{-3}$ μm (Clark et al., 2013), $\rho_m = 1.15 \times 10^{-6}$ $\mu\text{g } \mu\text{m}^{-3}$ (Raven, 1984), $g_{\text{dw}} = 0.47 \mu\text{g } \mu\text{g}^{-1}$ (Reynolds, 2006), and $\rho_{\text{cell}} = 10^{-6} \mu\text{g } \mu\text{m}^{-3}$ (Clark et al., 2013).

Appendix B: Downregulation of Nutrient Uptake

A cell of the size class i reduces its nutrient uptake by a factor $\rho_{\text{N},i}$ under light limitation to restrict the excess nutrient uptake. There will be no excretion of nutrient when the flux of carbon $(1 - \beta_{\text{L}})J_{\text{L},i} + (c_{\text{CN}} - \beta_{\text{F}})J_{\text{F},i}$ and nutrient $\rho_{\text{N},i}J_{\text{N},i} + J_{\text{F},i}$ available for synthesis has the correct ratio to synthesize new biomass. The criterion for these two fluxes being compatible to create structure with C:N of c_{CN} is then

$$(1 - \beta_{\text{L}})J_{\text{L}} + (c_{\text{CN}} - \beta_{\text{F}})J_{\text{F}} - \beta_{\text{N}} \rho_{\text{N}} J_{\text{N}} - J_{\text{R}} = c_{\text{CN}}(\rho_{\text{N}} J_{\text{N}} + J_{\text{F}}), \quad (\text{B1})$$

which gives

$$\rho_{\text{N}} = \frac{J_{\text{L}} - \beta_{\text{L}} J_{\text{L}} - \beta_{\text{F}} J_{\text{F}} - J_{\text{R}}}{(\beta_{\text{N}} + c_{\text{CN}})J_{\text{N}}}. \quad (\text{B2})$$

Appendix C: Excretion of Nutrients

Cells excrete N in the environment when the flux of C available for synthesis is less than the available flux of N. Because of their ability to downregulate nutrient uptake under light-limited conditions, phototrophs, and generalist mixotrophs do not excrete N. However, since the C:N ratio of food is assumed fixed and heterotrophs have to spend C from there for respiratory purposes, they are always C limited and excrete excess N from the cell. Such a situation can also occur for obligate mixotrophs under light-limited conditions. The general formula for the rate of excretion of excess nutrient from a cell can be written as the difference between fluxes of N and C given by

$$N_{E,i} = J_{F,i} - \max \left[0, \frac{(1 - \beta_L)J_{L,i} + (c_{CN} - \beta_F)J_{F,i} - J_{R,i}}{c_{CN}} \right]. \quad (C1)$$

For heterotrophic organisms, $J_{L,i} = 0$.

Appendix D: Hydromechanical Setup

The seasonal variation of light intensity (W m^{-2}) at different latitudes is calculated using an astronomical formula and based on the geographical location and the local date and time. The attenuation of solar radiation due to cloud cover is taken care of by setting the fractional could cover to 0.2 (Atchison et al., 1993). As light penetrates the water column, it decays exponentially with an attenuation coefficient of 0.04 m^{-1} to account for the light absorption by water (Kim et al., 2015). Wind speed (10 m above surface) and air temperature (2 m above surface) also vary seasonally (Figure S2). The temperature in the deep ocean ($>3,000 \text{ m}$) generally stays below 4.39°C (Sweetman et al., 2017), and thus, we choose oceanic bottom layer temperature as 4°C irrespective of the season. Salinity throughout the water column, air pressure (2 m above surface), and relative humidity are assumed constant with values 34 Practical Salinity Unit (PSU) (Molland, 2008), 1,074 hectopascal (Alonso & Ledesma, 2005) and 70% (Molland, 2008), respectively.

Nutrient concentration in the deep ocean is considered constant ($280 \mu\text{g N L}^{-1}$), and the exchange of nutrients with the bottom layer happens at a constant rate ($S=0.2 \text{ m day}^{-1}$). We allow only detritus to sink at a constant speed of 5 m day^{-1} where other components do not sink in our model. We use uniform initial concentrations of nutrient, living organisms, and detritus at all latitudes as $150 \mu\text{g N L}^{-1}$, $0.2 \mu\text{g}$, and $0.2 \mu\text{g L}^{-1}$, respectively. The model runs for 10 years. The first 9 years are considered as spin-up to reach the realistic vertical profiles and the data from the tenth year is used for plots.

Acknowledgments

The Centre for Ocean Life is supported by the Villum Foundation. S. C. and M. C. were supported by the Gordon and Betty Moore Foundation through award #5479. J. B. was supported by the Marine Ecosystems Research Programme (NE/L003066/1) of the Natural Environment Research Council and the Department for Environment, Food and Rural Affairs (Defra), as well as NERC National Capability in Marine Modeling. The authors are grateful to Adam Martiny, the Associate Editor, Ben Ward, and one anonymous reviewer for their extremely valuable comments and suggestion on the previous version of the manuscript. Sources of all data used to tune parameters are provided in the caption of Figure S1. Data sets for this research are included in these papers (and their supporting information files) (Edwards et al., 2012, 2015; P. J. Hansen et al., 1997; Jakobsen & Markager, 2016; Kiørboe, 2011; Marañón et al., 2000, 2001, 2013; Mojica et al., 2015; Moloney & Field, 1989; van de Poll et al., 2013; Taguchi, 1976; B. A. Ward et al., 2012). General Ocean Turbulence Model is used as a framework for our coupled biological-physical model (Umlauf et al., 2005) combined with the Fortran-based Framework for Aquatic Biogeochemical Models (Bruggeman & Bolding, 2014). Codes for Figures 5 and 7 are available at DOI:10.11583/DTU.12310016 (<https://figshare.com/s/d5c8badb325e94d0df4a>).

References

- Acevedo-Trejos, E., Marañón, E., & Merico, A. (2018). Phytoplankton size diversity and ecosystem function relationships across oceanic regions. *Proceedings of the Biological Sciences*, 285(1879), 20180621. <https://doi.org/10.1098/rspb.2018.0621>
- Allen, A. P., Gillooly, J. F., & Brown, J. H. (2005). Linking the global carbon cycle to individual metabolism. *Functional Ecology*, 19(2), 202–213. <https://doi.org/10.1111/j.1365-2435.2005.00952.x> @10.1111/(ISSN)1365-2435.MAKINGTHEMOSTOFMICROBES
- Alonso, E. E., & Ledesma, A. (Eds.) (2005). *Advances in Understanding Engineered Clay Barriers: Proceedings of the International Symposium on Large Scale Field Tests in Granite, Sitges, Barcelona, Spain, 12–14 November 2003*. CRC Press.
- Andersen, K. H., Aksnes, D. L., Berge, T., Fiksen, Ø., & Visser, A. (2015). Modelling emergent trophic strategies in plankton. *Journal of Plankton Research*, 37(5), 862–868. <https://doi.org/10.1093/plankt/fbv054>
- Andersen, K. H., Berge, T., Gonçalves, R. J., Hartwig, M., Heuschele, J., Hylander, S., et al. (2016). Characteristic sizes of life in the oceans, from bacteria to whales. *Annual Review of Marine Science*, 8(1), 217–241. <https://doi.org/10.1146/annurev-marine-122414-034144>
- Atchison, M. K., Schumann, R., Taylor, G., Warburton, J., Wheeler, M., & Yersavich, A. (1993). Shuttle landing facility cloud cover study: Climatological analysis and two tenths cloud cover rule evaluation. Retrieved from <https://ntrs.nasa.gov/search.jsp?R=19930021844&terms=Shuttle+landing+facility+cloud+cover+study+Climatological+analysis+two+tenths+cloud+cover+rule+evaluation&qs=%N%3D0%26Ntk%3DAll%26Ntt%3DShuttle%2520landing%2520facility%2520cloud%2520cover%2520study%253A%2520Climatological%2520analysis%2520and%2520two%2520tenths%2520cloud%2520rule%2520evaluation%26Ntx%3Dmode%2520matchallpartial%26Nm%3D123%7CCollection%7CNASA%2520STI%7C%7C17%7CCollection%7CNACA>
- Banas, N. S. (2011). Adding complex trophic interactions to a size-spectral plankton model: Emergent diversity patterns and limits on predictability. *Ecological Modelling*, 222(15), 2663–2675. <https://doi.org/10.1016/j.ecolmodel.2011.05.018>
- Berge, T., Chakraborty, S., Hansen, P. J., & Andersen, K. H. (2017). Modeling succession of key resource-harvesting traits of mixotrophic plankton. *The ISME Journal*, 11(1), 212–223. <https://doi.org/10.1038/ismej.2016.92>
- Blackman, F. F. (1905). Optima and Limiting Factors. *Annals of Botany*, 19(2), 281–296. <https://doi.org/10.1093/oxfordjournals.aob.a089000>
- Boyd, P. W., & Newton, P. P. (1999). Does planktonic community structure determine downward particulate organic carbon flux in different oceanic provinces? *Deep Sea Research Part I: Oceanographic Research Papers*, 46(1), 63–91. [https://doi.org/10.1016/S0967-0637\(98\)00066-1](https://doi.org/10.1016/S0967-0637(98)00066-1)
- Bruggeman, J. (2009). An adapting ecosystem manoeuvring between autotrophy and heterotrophy. In *Succession in plankton communities: a trait-based perspective* (pp. 71–100) (Doctoral dissertation). Amsterdam, The Netherlands: Vrije Universiteit. <https://research.vu.nl/en/publications/selection-in-plankton-communities-a-trait-based-perspective>
- Bruggeman, J., & Bolding, K. (2014). A general framework for aquatic biogeochemical models. *Environmental Modelling & Software*, 61, 249–265. <https://doi.org/10.1016/j.envsoft.2014.04.002>
- Bruggeman, J., & Kooijman, S. A. L. M. (2007). A biodiversity-inspired approach to aquatic ecosystem modeling. *Limnology and Oceanography*, 52(4), 1533–1544. <https://doi.org/10.4319/lo.2007.52.4.1533>
- Brun, P., Stamieszkin, K., Visser, A. W., Licandro, P., Payne, M. R., & Kiørboe, T. (2019). Climate change has altered zooplankton-fuelled carbon export in the North Atlantic. *Nature Ecology & Evolution*, 3(3), 416–423. <https://doi.org/10.1038/s41559-018-0780-3>
- Burkholder, J. M., Glibert, P. M., & Skelton, H. M. (2008). Mixotrophy, a major mode of nutrition for harmful algal species in eutrophic waters. *Harmful Algae*, 8(1), 77–93. <https://doi.org/10.1016/j.hal.2008.08.010>

- Butenschön, M., Clark, J., Aldridge, J. N., Allen, J. I., Artioli, Y., Blackford, J., et al. (2016). ERSEM 15.06: A generic model for marine biogeochemistry and the ecosystem dynamics of the lower trophic levels. *Geoscientific Model Development*, 9(4), 1293–1339. <https://doi.org/10.5194/gmd-9-1293-2016>
- Cadier, M., Andersen, K. H., Visser, A. W., & Kiørboe, T. (2019). Competition-defense tradeoff increases the diversity of microbial plankton communities and dampens trophic cascades. *Oikos*, 128(7), 1027–1040. <https://doi.org/10.1111/oik.06101>
- Chakraborty, S., Nielsen, L. T., & Andersen, K. H. (2017). Trophic strategies of unicellular plankton. *The American Naturalist*, 189(4), E77–E90. <https://doi.org/10.1086/690764>
- Chisholm, S. W. (1992). Phytoplankton size. In P. G. Falkowski & A. D. Woodhead (Eds.), *Primary productivity and biogeochemical cycles in the sea* (pp. 213–237). New York: Plenum Press.
- Clark, J. R., Lenton, T. M., Williams, H. T. P., & Daines, S. J. (2013). Environmental selection and resource allocation determine spatial patterns in picophytoplankton cell size. *Limnology and Oceanography*, 58(3), 1008–1022. <https://doi.org/10.4319/lo.2013.58.3.1008>
- Edwards, K. F., Thomas, M. K., Klausmeier, C. A., & Litchman, E. (2012). Allometric scaling and taxonomic variation in nutrient utilization traits and maximum growth rate of phytoplankton. *Limnology and Oceanography*, 57(2), 554–566. <https://doi.org/10.4319/lo.2012.57.2.00554>
- Edwards, K. F., Thomas, M. K., Klausmeier, C. A., & Litchman, E. (2015). Light and growth in marine phytoplankton: Allometric, taxonomic, and environmental variation. *Limnology and Oceanography*, 60(2), 540–552. <https://doi.org/10.1002/lno.10033>
- Eppley, R. (1972). Temperature and phytoplankton growth in the sea. *Fishery Bulletin*, 70(4), 1063–1085. Retrieved from https://marine.rutgers.edu/pubs/private/fishery_bulletin/vol70/no4/1972.Pdf
- Flynn, K. J., Stoecker, D. K., Mitra, A., Raven, J. A., Glibert, P. M., Hansen, P. J., et al. (2013). Misuse of the phytoplankton-zooplankton dichotomy: The need to assign organisms as mixotrophs within plankton functional types. *Journal of Plankton Research*, 35(1), 3–11. <https://doi.org/10.1093/plankt/fbs062>
- Follows, M. J., Dutkiewicz, S., Grant, S., & Chisholm, S. W. (2007). Emergent biogeography of microbial. *Science*, 315(5820), 1843–1846. <https://doi.org/10.1126/science.1138544>
- Friedland, K. D., Stock, C., Drinkwater, K. F., Link, J. S., Leaf, R. T., Shank, B. V., et al. (2012). Pathways between primary production and fisheries yields of large marine ecosystems. *PLoS ONE*, 7(1), e28945. <https://doi.org/10.1371/journal.pone.0028945>
- Großkopf, T., & LaRoche, J. (2012). Direct and indirect costs of dinitrogen fixation in *Crocospaera watsonii* WH8501 and possible implications for the nitrogen cycle. *Frontiers in Microbiology*, 3, 236. <https://doi.org/10.3389/fmicb.2012.00236>
- Hansen, A. N., & Visser, A. W. (2016). Carbon export by vertically migrating zooplankton: An optimal behavior model. *Limnology and Oceanography*, 61(2), 701–710. <https://doi.org/10.1002/lno.10249>
- Hansen, A. N., & Visser, A. W. (2019). The seasonal succession of optimal diatom traits. *Limnology and Oceanography*, lno.11126. <https://doi.org/10.1002/lno.11126>
- Hansen, P. J., Bjørnsen, P. K., & Hansen, B. W. (1997). Zooplankton grazing and growth: Scaling within the 2–2,000- μ m body size range. *Limnology and Oceanography*, 42(4), 687–704. <https://doi.org/10.4319/lo.1997.42.4.00687>
- Hartmann, M., Grob, C., Tarhan, G. A., Martin, A. P., Burkhill, P. H., Scanlan, D. J., & Zubkov, M. V. (2012). Mixotrophic basis of Atlantic oligotrophic ecosystems. *Proceedings of the National Academy of Sciences of the United States of America*, 109(15), 5756–5760. <https://doi.org/10.1073/pnas.1118179109>
- Hutchinson, G. E. (1941). Ecological aspects of succession in natural populations. *The American Naturalist*, 75(760), 406–418. <https://doi.org/10.1086/280983>
- Finkel, Z. V., & Irwin, A. J. (2000). Modeling size-dependent photosynthesis: Light absorption and the Allometric rule. *Journal of Theoretical Biology*, 204(3), 361–369. <https://doi.org/10.1006/jtbi.2000.2020>
- Jakobsen, H. H., & Markager, S. (2016). Carbon-to-chlorophyll ratio for phytoplankton in temperate coastal waters: Seasonal patterns and relationship to nutrients. *Limnology and Oceanography*, 61(5), 1853–1868. <https://doi.org/10.1002/lno.10338>
- Kemp, A. E., Pike, J., Pearce, R. B., & Lange, C. B. (2000). The “fall dump”—A new perspective on the role of a “shade flora” in the annual cycle of diatom production and export flux. *Deep Sea Research Part II: Topical Studies in Oceanography*, 47(9–11), 2129–2154. [https://doi.org/10.1016/S0967-0645\(00\)00019-9](https://doi.org/10.1016/S0967-0645(00)00019-9)
- Kim, G. E., Pradal, M. A., & Gnanadesikan, A. (2015). Quantifying the biological impact of surface ocean light attenuation by colored detrital matter in an ESM using a new optical parameterization. *Biogeosciences*, 12(16), 5119–5132. <https://doi.org/10.5194/bg-12-5119-2015>
- Kiørboe, T. (2011). How zooplankton feed: Mechanisms, traits and trade-offs. *Biological Reviews*, 86(2), 311–339. <https://doi.org/10.1111/j.1469-185X.2010.00148.x>
- Kiørboe, T., & Hirst, A. G. (2014). Shifts in mass scaling of respiration, feeding, and growth rates across life-form transitions in marine pelagic organisms. *The American Naturalist*, 183(4), E118–E130. <https://doi.org/10.1086/675241>
- Kustka, A., Carpenter, E. J., & Sañudo-Wilhelmy, S. A. (2002). Iron and marine nitrogen fixation: Progress and future directions. *Research in Microbiology*, 153(5), 255–262. [https://doi.org/10.1016/S0923-2508\(02\)01325-6](https://doi.org/10.1016/S0923-2508(02)01325-6)
- Lavrentyev, P., & Franzé, G. (2017). *CarbonBridge May 2014: Microzooplankton biomass distribution in the waters northwest of Spitsbergen*. PANGAEA: University of Akron. Retrieved from: <https://doi.org/10.1594/PANGAEA.881808>
- Li, W. K. W. (1985). Photosynthetic response to temperature of marine phytoplankton along a latitudinal gradient (16°N to 74°N). *Deep Sea Research Part A: Oceanographic Research Papers*, 32(11), 1381–1391. [https://doi.org/10.1016/0198-0149\(85\)90054-8](https://doi.org/10.1016/0198-0149(85)90054-8)
- Lindemann, C., Fiksen, Ø., Andersen, K. H., & Aksnes, D. L. (2016). Scaling laws in phytoplankton nutrient uptake affinity. *Frontiers in Marine Science*, 3, 26. <https://doi.org/10.3389/fmars.2016.00026>
- Litchman, E., & Klausmeier, C. A. (2008). Trait-based community ecology of phytoplankton. *Annual Review of Ecology, Evolution, and Systematics*, 39(1), 615–639. <https://doi.org/10.1146/annurev.ecolsys.39.110707.173549>
- López-Urrutia, A., San Martin, E., Harris, R. P., & Irigoien, X. (2006). Scaling the metabolic balance of the oceans. *Proceedings of the National Academy of Sciences of the United States of America*, 103(23), 8739–8744. <https://doi.org/10.1073/pnas.0601137103>
- Marañón, E. (2015). Cell size as a key determinant of phytoplankton metabolism and community structure. *Annual Review of Marine Science*, 7(1), 241–264. <https://doi.org/10.1146/annurev-marine-010814-015955>
- Marañón, E., Cermeño, P., López-Sandoval, D. C., Rodríguez-Ramos, T., Sobrino, C., Huete-Ortega, M., et al. (2013). Unimodal size scaling of phytoplankton growth and the size dependence of nutrient uptake and use. *Ecology Letters*, 16(3), 371–379. <https://doi.org/10.1111/ele.12052>
- Marañón, E., Holligan, P. M., Barciela, R., González, N., Mouríño, B., Pazó, M. J., & Varela, M. (2001). Marañón 2001 phytoplankton size structure in contrasting ocean environs. *Marine Ecology Progress Series*, 216, 43–56. <https://doi.org/10.3354/meps216043>

- Marañón, E., Holligan, P. M., Varela, M., Mouríño, B., & Bale, A. J. (2000). Basin-scale variability of phytoplankton biomass, production and growth in the Atlantic Ocean. *Deep Sea Research Part I: Oceanographic Research Papers*, 47(5), 825–857. [https://doi.org/10.1016/s0967-0637\(99\)00087-4](https://doi.org/10.1016/s0967-0637(99)00087-4)
- Masojidek, J., Torzillo, G., Kobližek, M., Kopecký, J., Bernardini, P., Sacchi, A., & Komenda, J. (1999). Photoadaptation of two members of the chlorophyta (*scenedesmus* and *chlorella*) in laboratory and outdoor cultures: Changes in chlorophyll fluorescence quenching and the xanthophyll cycle. *Planta*, 209(1), 126–135. <https://doi.org/10.1007/s004250050614>
- Mojica, K. D. A., van de Poll, W. H., Kehoe, M., Huisman, J., Timmermans, K. R., Buma, A. G. J., et al. (2015). Phytoplankton community structure in relation to vertical stratification along a north-south gradient in the Northeast Atlantic Ocean. *Limnology and Oceanography*, 60(5), 1498–1521. <https://doi.org/10.1002/lno.10113>
- Molland, A. (2008). *The maritime engineering reference book: A guide to ship design, construction and operation*. Oxford, UK: Butterworth-Heinemann.
- Moloney, C. L., & Field, J. G. (1989). General allometric equations for rates of nutrient uptake, ingestion, and respiration in plankton organisms. *Limnology and Oceanography*, 34(7), 1290–1299. <https://doi.org/10.4319/lo.1989.34.7.1290>
- Morel, A., & Bricaud, A. (1981). Theoretical results concerning light absorption in a discrete medium, and application to specific absorption of phytoplankton. *Deep Sea Research Part A. Oceanographic Research Papers*, 28(11), 1375–1393. [https://doi.org/10.1016/0198-0149\(81\)90039-X](https://doi.org/10.1016/0198-0149(81)90039-X)
- Munk, W., & Riley, G. (1952). Absorption of nutrients by aquatic plants. *Journal of Marine Research*, 11, 215–240.
- Norberg, J., Swaney, D. P., Dushoff, J., Lin, J., Casagrandi, R., & Levin, S. A. (2001). Phenotypic diversity and ecosystem functioning in changing environments: A theoretical framework. *Proceedings of the National Academy of Sciences*, 96(4), 1463–1468. <https://doi.org/10.1073/pnas.96.4.1463>
- Orth, J. D., Thiele, I., & Palsson, B. Ø. (2010). What is flux balance analysis? *Nature Biotechnology*, 28(3), 245–248. <https://doi.org/10.1038/nbt.1614>
- Oschlies, A. (2002). Nutrient supply to the surface waters of the North Atlantic: A model study. *Journal of Geophysical Research*, 107(C5), 3046. <https://doi.org/10.1029/2000JC000275>
- Platt, T., Gallegos, C. L., & Harrison, W. G. (1980). Photoinhibition of photosynthesis in natural assemblages of marine-phytoplankton. *Journal of Marine Research*, 38, 687–701.
- Raven, J. A. (1984). A cost-benefit analysis of photon absorption by photosynthetic unicells. *New Phytologist*, 98(4), 593–625. <https://doi.org/10.1111/j.1469-8137.1984.tb04152.x>
- Raven, J., & Geider, R. (1988). Temperature and algal growth. *New Phytologist*, 110(4), 441–461. <https://doi.org/10.1111/j.1469-8137.1988.tb00282.x>
- Redfield, A. C. (1958). The biological control of chemical factors in the environment. *American Scientist*, 46, 205–221.
- Reynolds, C. (2006). *The ecology of phytoplankton*. Cambridge, UK: Cambridge University Press.
- Rose, J. M., & Caron, D. A. (2007). Does low temperature constrain the growth rates of heterotrophic protists? Evidence and implications for algal blooms in cold waters. *Limnology and Oceanography*, 52(2), 886–895. <https://doi.org/10.4319/lo.2007.52.2.00886>
- Ryther, J. H. (1969). Photosynthesis and fish production in the sea. *Science*, 166(3901), 72–76. <https://doi.org/10.1126/science.166.3901.72>
- Sanders, R. W. (1991). Mixotrophic protists in marine and freshwater ecosystems. *The Journal of Protozoology*, 38(1), 76–81. <https://doi.org/10.1111/j.1550-7408.1991.tb04805.x>
- Sanders, R. W., & Gast, R. J. (2012). Bacterivory by phototrophic picoplankton and nanoplankton in Arctic waters. *FEMS Microbiology Ecology*, 82(2), 242–253. <https://doi.org/10.1111/j.1574-6941.2011.01253.x>
- Sanders, R. W., Henson, S. A., Koski, M., De La Rocha, C. L., Painter, S. C., Poulton, A. J., et al. (2014). The biological carbon pump in the North Atlantic. *Progress in Oceanography*, 129, 200–218. <https://doi.org/10.1016/J.POCEAN.2014.05.005>
- Serra-Pompeii, C., Hagstrom, G. I., Visser, A. W., & Andersen, K. H. (2019). Resource limitation determines temperature response of unicellular plankton communities. *Limnology and Oceanography*, 64(4), 1627–1640. <https://doi.org/10.1002/lno.11140>
- Smetacek, V. (1999). Diatoms and the ocean carbon cycle. *Protist*, 150(1), 25–32. [https://doi.org/10.1016/S1434-4610\(99\)70006-4](https://doi.org/10.1016/S1434-4610(99)70006-4)
- Smith, R. E. H., & Kalf, J. (1983). Competition for phosphorus among co-occurring freshwater phytoplankton. *Limnology and Oceanography*, 28(3), 448–464. <https://doi.org/10.4319/lo.1983.28.3.0448>
- Smith, S. L., Pahlow, M., Merico, A., Acevedo-Trejos, E., Sasai, Y., Yoshikawa, C., et al. (2016). Flexible phytoplankton functional type (FlexPFT) model: Size-scaling of traits and optimal growth. *Journal of Plankton Research*, 38(4), 977–992. <https://doi.org/10.1093/plankt/fbv038>
- Sommer, U. (1983). Nutrient competition between phytoplankton species in multispecies chemostat experiments. *Archiv für Hydrobiologie*, 96, 399–416. Retrieved from <http://eprints.uni-kiel.de/14164/1/Nutrient.pdf>
- St. John, M. A., Borja, A., Chust, G., Heath, M., Grigorov, I., Mariani, P., et al. (2016). A dark hole in our understanding of marine ecosystems and their services: Perspectives from the mesopelagic community. *Frontiers in Marine Science*, 3, 31. <https://doi.org/10.3389/fmars.2016.00031>
- Steinberg, D. K., & Landry, M. R. (2017). Zooplankton and the ocean carbon cycle. *Annual Review of Marine Science*, 9(1), 413–444. <https://doi.org/10.1146/annurev-marine-010814-015924>
- Stoecker, D., Johnson, M., de Vargas, C., & Not, F. (2009). Acquired phototrophy in aquatic protists. *Aquatic Microbial Ecology*, 57(3), 279–310. <https://doi.org/10.3354/ame01340>
- Sweetman, A. K., Thurber, A. R., Smith, C. R., Levin, L. A., Mora, C., Wei, C.-L., et al. (2017). Major impacts of climate change on deep-sea benthic ecosystems. *Elem Sci Anth*, 5(0), 4. <https://doi.org/10.1525/elementa.203>
- Taguchi, S. (1976). Relationship between photosynthesis and cell size of marine diatoms. *Journal of Phycology*, 12, 185–189.
- Taylor, A., & Landry, M. (2018). Phytoplankton biomass and size structure across trophic gradients in the southern California current and adjacent ocean ecosystems. *Marine Ecology Progress Series*, 592, 1–17. <https://doi.org/10.3354/meps12526>
- Terseleer, N., Bruggeman, J., Lancelot, C., & Gypens, N. (2014). Trait-based representation of diatom functional diversity in a plankton functional type model of the eutrophied southern North Sea. *Limnology and Oceanography*, 59(6), 1958–1972. <https://doi.org/10.4319/lo.2014.59.6.1958>
- Thingstad, T. F., & Aksnes, D. L. (2019). Why growth of nutrient-limited micro-organisms should have low-temperature sensitivity. *The ISME Journal*, 13(2), 557–558. <https://doi.org/10.1038/s41396-018-0271-1>
- Thingstad, T. F., Øvreås, L., Egge, J. K., Løvdal, T., & Heldal, M. (2005). Use of non-limiting substrates to increase size; a generic strategy to simultaneously optimize uptake and minimize predation in pelagic osmotrophs? *Ecology Letters*, 8(7), 675–682. <https://doi.org/10.1111/j.1461-0248.2005.00768.x>

- Tréguer, P. J., & De La Rocha, C. L. (2013). The world ocean silica cycle. *Annual Review of Marine Science*, 5(1), 477–501. <https://doi.org/10.1146/annurev-marine-121211-172346>
- Uitz, J., Claustre, H., Gentili, B., & Stramski, D. (2010). Phytoplankton class-specific primary production in the world's oceans: Seasonal and interannual variability from satellite observations. *Global Biogeochemical Cycles*, 24, 1–19. <https://doi.org/10.1029/2009GB003680>
- Umlauf, L., Burchard, H., & Bolding, K. (2005). General ocean turbulence model. In *Source code documentation. Baltic Sea Research Institute Warnemünde Technical Report* (Vol. 63, 346 pp.).
- van de Poll, W. H., Kulk, G., Timmermans, K. R., Brussaard, C. P. D., van der Woerd, H. J., Kehoe, M. J., et al. (2013). Phytoplankton chlorophyll *a* biomass, composition, and productivity along a temperature and stratification gradient in the northeast Atlantic Ocean. *Biogeosciences*, 10, 4227–4240. <https://doi.org/10.5194/bg-10-4227-2013>
- Ward, B. A., Dutkiewicz, S., Jahn, O., & Follows, M. J. (2012). A size-structured food-web model for the global ocean. *Limnology and Oceanography*, 57(6), 1877–1891. <https://doi.org/10.4319/lo.2012.57.6.1877>
- Ward, B. A., & Follows, M. J. (2016). Marine mixotrophy increases trophic transfer efficiency, mean organism size, and vertical carbon flux. *Proceedings of the National Academy of Sciences of the United States of America*, 113(11), 2958–2963. <https://doi.org/10.1073/pnas.1517118113>
- Westoby, M., & Wright, I. J. (2006). Land-plant ecology on the basis of functional traits. *Trends in Ecology & Evolution*, 21(5), 261–268. <https://doi.org/10.1016/j.tree.2006.02.004>
- Wilken, S., Huisman, J., Naus-Wiezer, S., & Van Donk, E. (2013). Mixotrophic organisms become more heterotrophic with rising temperature. *Ecology Letters*, 16(2), 225–233. <https://doi.org/10.1111/ele.12033>
- Wirtz, K.-W., & Eckhardt, B. (1996). Effective variables in ecosystem models with an application to phytoplankton succession. *Ecological Modelling*, 92(1), 33–53. [https://doi.org/10.1016/0304-3800\(95\)00196-4](https://doi.org/10.1016/0304-3800(95)00196-4)
- Yool, A., Popova, E. E., & Anderson, T. R. (2013). MEDUSA-2.0: An intermediate complexity biogeochemical model of the marine carbon cycle for climate change and ocean acidification studies. *Geoscientific Model Development*, 6(5), 1767–1811. <https://doi.org/10.5194/gmd-6-1767-2013>
- Zubkov, M. V., & Tarhan, G. A. (2008). High bacterivory by the smallest phytoplankton in the North Atlantic Ocean. *Nature*, 455(7210), 224–226. <https://doi.org/10.1038/nature07236>